Neither too little nor too much: finding the ideal proportion of excipients

Hery Mitsutake[‡,§]*, Gustavo H. Rodrigues da Silva*[‡], *Márcia C. Breitkreitz*[†], *Eneida de Paula*[‡], *Heloisa N. Bordallo*[§]

* Corresponding Author

AUTHOR ADDRESS:

Author: Hery Mitsutake

Affiliation:

[‡]Department of Biochemistry and Tissue Biology, Institute of Biology, Unicamp. Rua Monteiro Lobato, 255. bloco F sup., sala 9, Campinas, SP, Brazil. 13083-862.

[§] Niels Bohr Institute, University of Copenhagen, Universitetsparken 5, 2100 Copenhagen, Denmark

E-mail: herymitsutake@gmail.com; ORCID: https://orcid.org/0000-0002-8769-0301

Author: Gustavo H. Rodrigues da Silva

Affiliation: [‡] Department of Biochemistry and Tissue Biology, Institute of Biology, Unicamp. Rua Monteiro Lobato, 255. bloco F sup., sala 9, Campinas, SP, Brazil. 13083-862.

E-mail: gustavohrs@gmail.com ORCID: https://orcid.org/0000-0001-7377-8532

Author: Márcia C. Breitkreitz

Affiliation: [†]Department of Analytical Chemistry, Institute of Chemistry, Unicamp, Rua Josué de Castro, s/n Cid. Universitária Zeferino Vaz, Campinas, SP, Brazil. 13084-970.

E-mail: marciacb@unicamp.br ORCID: https://orcid.org/0000-0002-0596-9692

Author: Eneida de Paula

Affiliation: [‡] Department of Biochemistry and Tissue Biology, Institute of Biology, Unicamp. Rua Monteiro Lobato, 255. bloco F sup., sala 9, Campinas, SP, Brazil. 13083-862.

E-mail: depaula@unicamp.br ORCID: https://orcid.org/0000-0003-4504-5723

Author: Heloisa N. Bordallo

Affiliation: [§]Niels Bohr Institute, University of Copenhagen, Universitetsparken 5, 2100 Copenhagen, Denmark

E-mail: bordallo@nbi.ku.dk ORCID: https://orcid.org/0000-0003-0750-0553

KEYWORDS. butamben, homogeneity, DHI, Raman mapping, 3D image analysis.

ABSTRACT

Excipient's homogeneity is of paramount importance during the development of pharmaceutical formulations due to its relation to stability, safety and efficacy. A direct and unique approach to evaluate such property is 3D Raman imaging. This technique characterizes the surface and inner part of preformulation samples, allowing to determine phase separation in the early stages of pharmaceutical development. Aiming to promote controlled release of the local anesthetic butamben (BTB), confocal 3D Raman microscopy was used to obtain its optimal proportion in Apifil®, Capryol® 90 and Transcutol®. Even if the microscopic images of some samples displayed very homogeneous surfaces, analysis of 3D maps showed that chemical distribution throughout the material was different. To investigate how concentration affects the homogeneity, mixture experimental design (DoE) was employed. From this analysis, it was revealed that correct amount of Capryol® 90 enhances both miscibility and solubility. Furthermore, suitable miscibility was observed in two ratio proportions of excipients: Solution 1: Apifil® 30.00%, Capryol 20.00% and Transcutol 10.00% (w/w), with a desirability of 0.783; and Solution 2: Apifil® 25.00%, Capryol 25.00% and Transcutol 10.00% (w/w), with 0.742 desirability. These results unequivocally demonstrated that confocal Raman microscopy combined to DoE can bring pharmaceutical development to a higher level.

GRAPHICAL ABSTRACT

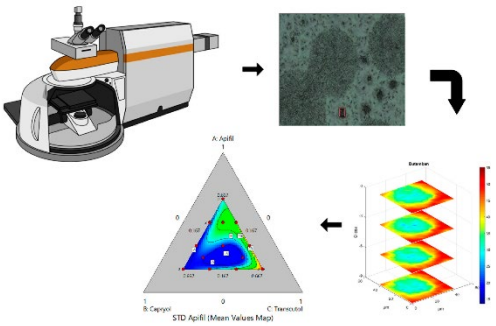

1. INTRODUCTION

Local anesthetics (LAs) originate from the leaves of a South American indigenous plant (*Erythroxylon coca*). LAs are used to attenuate or eliminate local pain in medical and dental procedures through various routes of administration, such as injective, topical, dermal and mucosal. Identification of the active principle of *Erythroxylon coca (*the alkaloid cocaine) led to the synthesis of numerous benzoic acid derivatives, such as benzocaine and butamben. Nowadays, aminoester and aminoamides are the most common families of clinically used LAs,[1,2] generally formed by an aromatic ring plus an intermediate amide chain. Changes in these portions modify the lipid/water distribution coefficient and the protein-binding characteristics, and in turn, markedly alter the anesthetic potency.[2]

In dentistry, topical anesthetics are widely applied for pain management, including benzocaine and butamben (BTB). However, anesthesia failure is a well-known effect in patients with acute endodontic pain. To overcome this challenge, encapsulation of BTB in lipid carriers was shown to promote controlled release and enhance its efficacy without inducing any side effects.[3,4] Nonetheless, further improvements on the global miscibility of these drug delivery systems (DDS) are still needed. However, achieving formulation homogeneity, and consequently,

stability, safety and efficacy can be challenging.[5] In the case of BTB, obtaining a homogenous mixture with lipidic excipients is not straightforward since it belongs to BCS (Biopharmaceutical Classification System) Class II, however it presents the "brick dust" behavior, i.e. even though it is poorly water soluble, it also presents poor solubility in lipids.[6]

Homogeneity can be evaluated either in a macroscopic way, by visual inspection and using microscopic imaging, especially chemical imaging methods that allow evaluating the chemical distribution.[7–9] . To this end, the non-destructive, label-free and reagent (solvent)-free inherent features of infrared spectroscopy and Raman scattering enables identifying ingredient distribution, providing for the optimization of the final product quality. Several methods were developed to analyze the chemical images, such as the distributional homogeneity index (DHI, an index based in macropixels and continuous-level moving block)[10], Poole-index (where the algorithm binarized the maps and works with non-overlapping macropixels)[11] and variographic analysis (where the variance values are estimated by comparing pairs of observations at different lags)[12], which have brought progress in describing sample homogeneity.[13,14] For instance, Ma *et al.*[15] have successfully used near infrared (NIR) images and DHI to evaluate the homogeneity of commercial chlorpheniramine maleate tablets. Mitsutake *et al.*[16] used Raman imaging and DHI to compare the homogeneity of natural and synthetic lipid in mixtures used to do nanostructured lipid carriers (NLC). More recently, our research group showed that 3D images might be required for visualizing drug overload when surface analysis is not sufficient.[6]

In particular, Raman confocal microscopy enables 3D images acquisition that can be crucial in some situations, including pharmacological, biological and pharmaceutical studies. For instance, Gotter *et al.*[17] applied this approach to follow the dithranol (antipsoriasis) diffusion in artificial acceptor membranes using semisolid formulations, while Chen *et al.*[18] tracked the fate of

the anticancer drug cisplatin in cells, proving the great potential of this technique for theragnostic purposes. Likewise, mycobacterial infections in zebrafish embryos as well the distribution of proteins, lipids, carotenoids and tissue characterization were successfully imaged by Raman confocal microscopy.[19]

In this work we discuss the power of confocal 3D Raman images in the development of new lipidic pharmaceutical formulations by determining changes in miscibility at the surface and in the inner parts of a new DDS designed for BTB. In addition, mixture design of experiments led to the determination of suitable proportions between API and excipients.

2. EXPERIMENTAL SECTION

2.1. Raw Material

Butamben (butyl 4-aminobenzoate, hereafter BTB) was purchased from Fluka Analytical (≥ 98.0%, w/w). Apifil® GC, the first wax derivative created by Gattefossé, based on beeswax and functionalized with polyethylene glycol-8, Capryol® 90, (propylene glycol monocaprylate) is a nonionic water-insoluble surfactant that can be used as cosurfactant, and Transcutol® GC, (diethylene glycol monoethyl ether), a solvent and solubilizer used for enhancing solubility and bioavailability in oral and alternative routes were donated by Gattefossé (France). All samples were analyzed as received.

2.2. Pre-formulation preparation method: Simplex-Lattice Mixture Design of Experiments

Simplex-lattice mixture design of experiments (DoE) was employed to develop the DDS studied here. BTB concentration was fixed at 40.00% (w/w), while the excipients concentration

range varied between 10.00 to 40.00% (w/w) as shown in Table 1, where the data is organized by Capryol® 90 concentration.

The sample preparation consisted of heating the solid excipient, Apifil®, 10ºC above its melting point ($T_{melting}$ = 59 ºC) and keeping the sample at this temperature until it was completely melted. Then, BTB was added to the mixture of liquid excipients, Capryol® 90 and Transcutol®, under stirring conditions until a visually homogeneous mixture was obtained. Afterwards, this mixture was added into the heated solid lipid, and mixed again. The obtained samples were deposited in Petri dishes and kept at room temperature (25 ± 1 ºC).

Table 1. Composition of the pre-formulation samples in the mixture DoE. Run refers to the random order of image acquisition.

Sample	Run	Apifil® Concentration*	Capryol Concentration*	Transcutol Concentration *
AM3	11	10.00	10.00	40.00
AM16	1	10.00	10.00	40.00
AM8	15	20.00	10.00	30.00
AM5	10	30.00	10.00	20.00
AM1	7	40.00	10.00	10.00
AM14	2	40.00	10.00	10.00
AM13	16	15.00	15.00	30.00
AM11	5	30.00	15.00	15.00
AM10	13	10.00	20.00	30.00
AM7	12	20.00	20.00	20.00
AM4	8	30.00	20.00	10.00
AM17	17	30.00	20.00	10.00
AM9	4	10.00	30.00	20.00
AM12	3	15.00	30.00	15.00
AM6	9	20.00	30.00	10.00
AM2	14	10.00	40.00	10.00
AM15	6	10.00	40.00	10.00

* % (w/w)

2.3. Raman Confocal Imaging

Raman volumetric images were collected using the inVia^{TM} confocal Raman microscope and the Wire v. 5.4 software (Renishaw, Gloucestershire, UK). The samples were deposited on Petri dishes and exposed to a laser excitation of 785 nm, laser power of 10 mW, dispersed by a 1200 lines/mm grating, CCD detector, spectral range from 715 to 1806 cm^{-1} and exposition for 1 sec. A 50× long distance (N.A. 0.50) objective was used giving a spatial resolution of 10 μm and 0.6 μm of depth of focus. Cube of data ($X \times Y \times Z \times \lambda$, where X, Y and Y are the pixel numbers in x, y and z axis and λ is the number of Raman shifts) with dimensions ranging from 15×15×4×1015 to 30×30×4×1015 were obtained. The step size at x, y and z axis was 3 μm. To avoid excess time consuming to map all surfaces, acquisition time between 2 to 3 hours, were obtained for each sample from Table 1.

Cosmic rays were excluded from the Raman spectra using the algorithm developed by Sabin *et al*.[20] The data cube was unfolded to a 2D matrix and asymmetric least squares were used for baseline correction. All spectra were normalized using unit vectors. Preprocessing was performed using Matlab version 8.3 (Mathworks Inc., Natick MA, USA) and PLS toolbox version 8.6.2 (Eigenvector Research Inc., Wenatchee, WA, USA).

2.4. Chemometric Analysis – Chemical Maps Using Classical Least Squares (CLS) and Mixture DoE

Prior to the chemometrics analysis, Raman spectra of the pure compounds and mean spectra from the maps were compared. As no changes in the spectral features were observed, such

as new peaks or their disappearance, the use of CLS is justified.[21] This algorithm is based on the bilinear model shown in Equation 1:

$$D = CS^T \quad (1)$$

where: **D** (XYZ × λ) is 2D matrix with sample spectra, **C** (XYZ × A) contains scores related with the compound concentrations, $\mathbf{S}^T$ (A × λ) contains the spectra of the pure compounds and A is the number of components, which in our case is 4.

Subsequently, chemical maps were obtained by refolding scores. DHI was calculated in 'extended maps' where each layer was added one after the other (Figure 1). First, the distribution map was built by all possible macropixels of 2 × 2 original pixel size, this step was repeated until there was a single macropixel of size equal to that of the whole distribution map. The standard deviation was calculated for each macropixel size and plotted against its size, generating the homogeneity curve. Then the distribution map was randomized, and the homogeneity curve computed. DHI is given by the ratio between original map and random maps. The randomization step was repeated 100 times.[10]

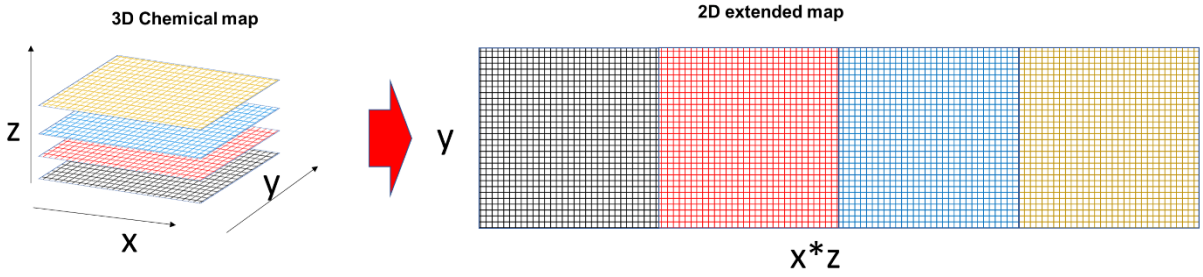

Figure 1. Conversion from 3D chemical map (X × Y × Z) to 2D (XZ × Y) extended map used for the DHI calculations.

Each map gave a histogram of CLS scores frequency where mean values for each compound could be extracted. The standard deviation was calculated from the mean values obtained for each map (STD_{maps}). STD_{maps} from different regions for the same sample were used as input for mixture DoE. If the sample is heterogeneous, a high STD_{maps} value for the surface analysis will be obtained, while for extended 2D maps the DHI is larger than in cases of similar concentrations in different layers.

CLS models were built using Matlab version 8.3 (Mathworks Inc., Natick MA, USA) and PLS_toolbox version 8.6.2 (Eigenvector Research Inc., Wenatchee, WA, USA). The mixture DoE models and regression analysis were carried out using Design Expert version 11 (Stat-Ease Inc., Minneapolis, MN, USA). Significance level was 0.05 for all analysis.

3. RESULTS AND DISCUSSION

3.1. Microscopic inspection and 3D Raman imaging analysis

Figure 2 shows the mean spectra of each map of sample AM1 (Table 1), compared to the pure compound spectrum, in order to identify new peaks or changes in Raman shift. As explained in Materials and Methods Section, CLS can be employed in this case because no changes in the spectral features were observed.

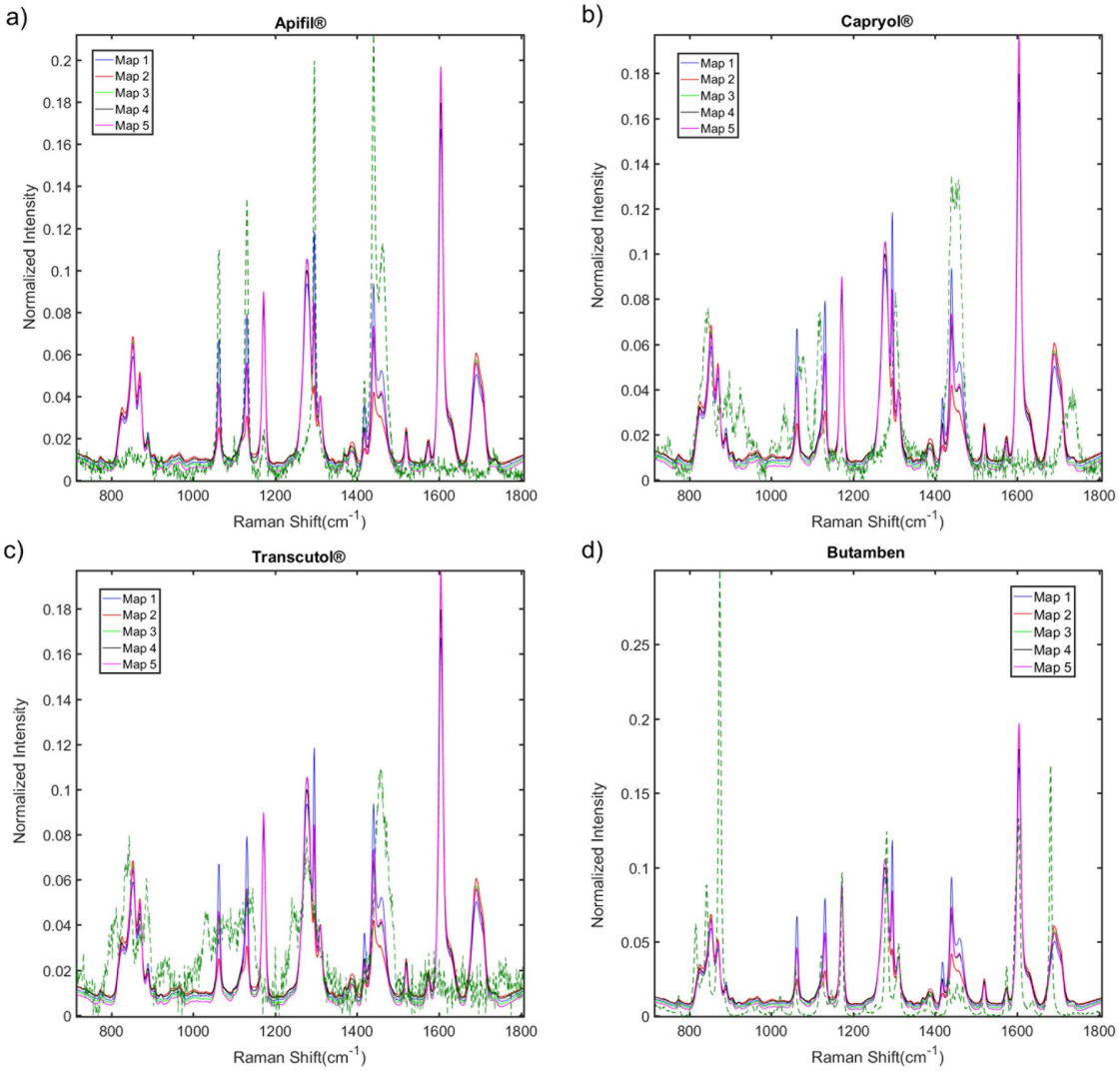

Figure 2. Comparison between pure compound spectrum (----) and mean spectra from Raman maps taken for the sample AM1 (see Table 1) for: a) Apifil®, b) Capryol® 90, c) Transcutol® and d) BTB.

As shown in Figure 2, other than the vibration at 1600 cm^{-1}, unique to BTB and assigned to C=C in the aromatic ring and N-H bond,[22] there were no selective regions to build univariate maps of excipients. This implies that the use of multivariate models was the most suitable way to obtain 3D chemical maps for each sample. Nevertheless, before proceeding with the image

analysis, we will discuss the results based on a visual inspection of the visible images obtained by confocal microscopy, as shown in Figure 3 and Figure S1 (Supporting Information). This simple approach allowed us to divide the samples into 3 groups:

(i) Very heterogeneous, group 1: samples AM5, AM8 and AM16 showed a heterogeneous surface with darker and rougher regions (Figure 3a). These were the samples with the lowest Capryol® 90 concentration. Samples AM1 and AM3, with 10% w/w of the liquid lipid also have some heterogeneities in the surface.

(ii) Homogeneous with smoother surfaces, group 2: samples AM2, AM6, AM7, AM9, AM10, AM12, AM13 and AM15, which contain until 20.00% (w/w) of Caproyl® 90, showed homogeneous and smoother surfaces (Figure 3b). Despite this, black spots in samples AM6 and AM7 might be a representation of different compositions.

(iii) Homogeneous with rougher surfaces, group 3: Samples AM4, AM11, AM14 and AM17, prepared with more than 30.00% (w/w) of Apifil® and lower concentrations of Transcutol®, have homogeneous but rougher surfaces than the previous ones (Figure 3c).

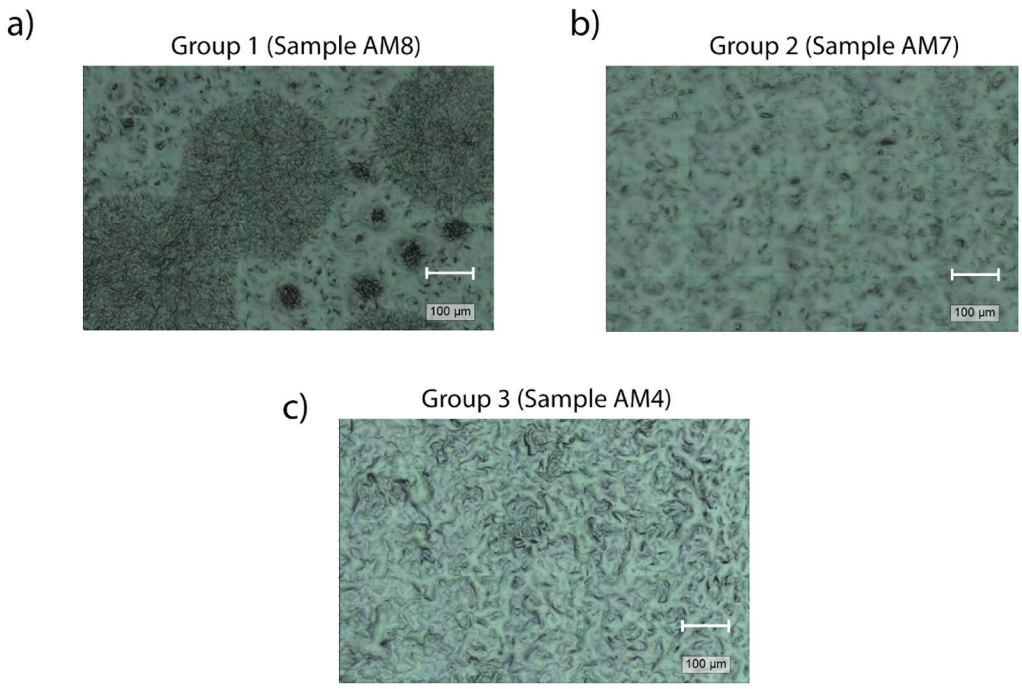

Figure 3. Confocal visible microscopic images from selected samples representing the 3 groups: a) very heterogeneous (AM8), b) homogeneous and smooth surface (AM7) and c) homogeneous and rough surface (Scale bar = 100µm).

Group 1 – Heterogenous surface and depth distribution.

Chemical maps from a representative region of sample AM8 are shown in Figure 4.

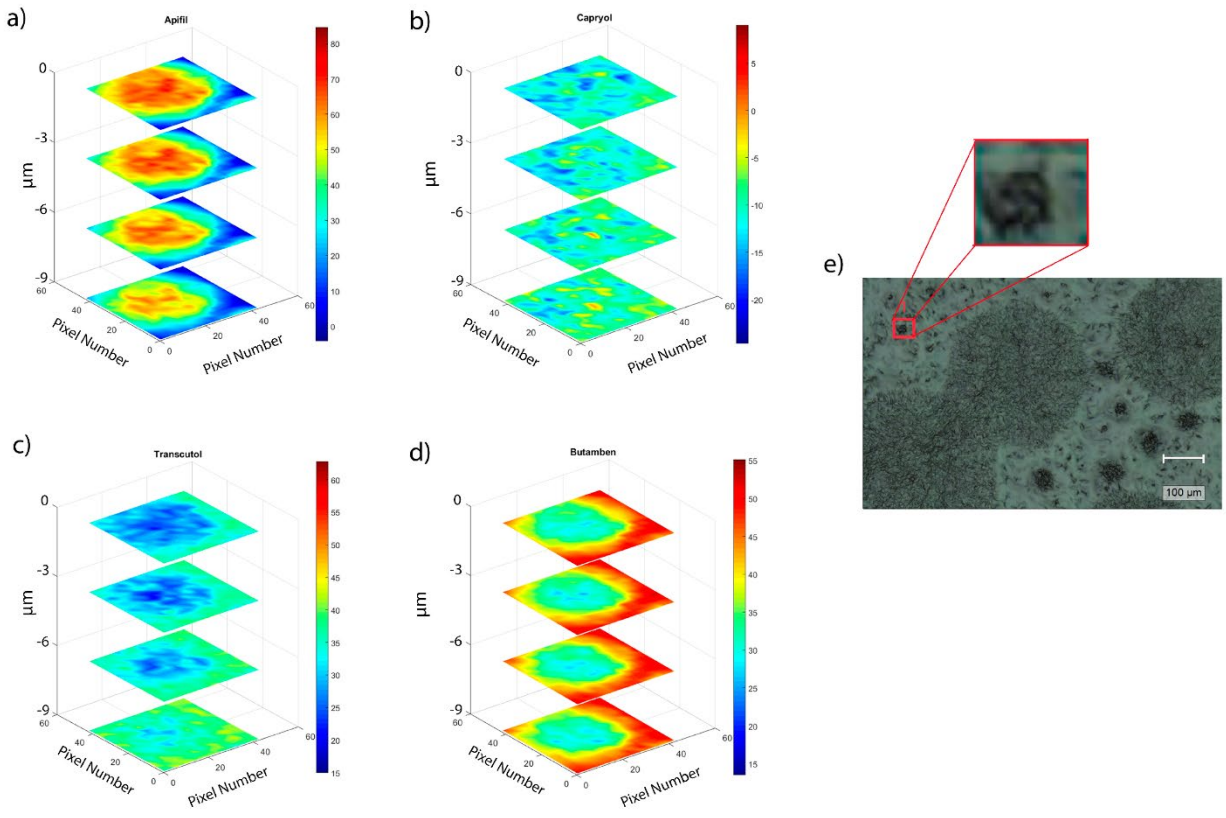

Figure 4. Volumetric Raman images obtained for a sample belongs to the very heterogeneous category (AM8) in the selected region 1 (red square in (e)) for: a) Apifil®, b) Capryol® 90, c) Transcutol® and d) BTB (Scale bar = 100µm, *x* axis = 560 µm, *y* axis = 860 µm).

For sample AM8, maps in region 1 (Figure 4) and region 3 (Figure S4) (the black spots observed in the surface and highlighted in the inset of Figure 4e and Figure S4e (Supporting Information) were basically composed of pure Apifil®. However, there is a clear difference of composition below −6 µm: Apifil® is more concentrated in the surface (red) than inside the sample (yellow). On the other hand, the other excipients (Capryol® 90 and Transcutol®) are more concentrated in the internal layers (blue outside and green inside) (Figure 4). More homogeneous regions were also found in this sample and are represented in regions 4 and 5 (Figure S5 and S6). Surprisingly, concentration differences when comparing different depths were also detected in

these parts. For example, BTB and Apifil® have hotter colors from −3 µm and above and the inverse is true for the liquid compounds. All this information gives clear indications of phase separation, with solid compounds located closer to the surface. In addition, the histograms of the region 1 are shown in Figure S2, where the heterogeneity of Apifil and BTB is highlighted when compared with Capryol® 90. Observing Table 1, the samples in this group have the lowest Capryol® 90 concentrations, 10% (w/w).

Group 2 – Homogeneous and smooth surfaces, but heterogenous depth distribution.

Chemical maps from a representative region of sample AM7 are shown in Figure 5.

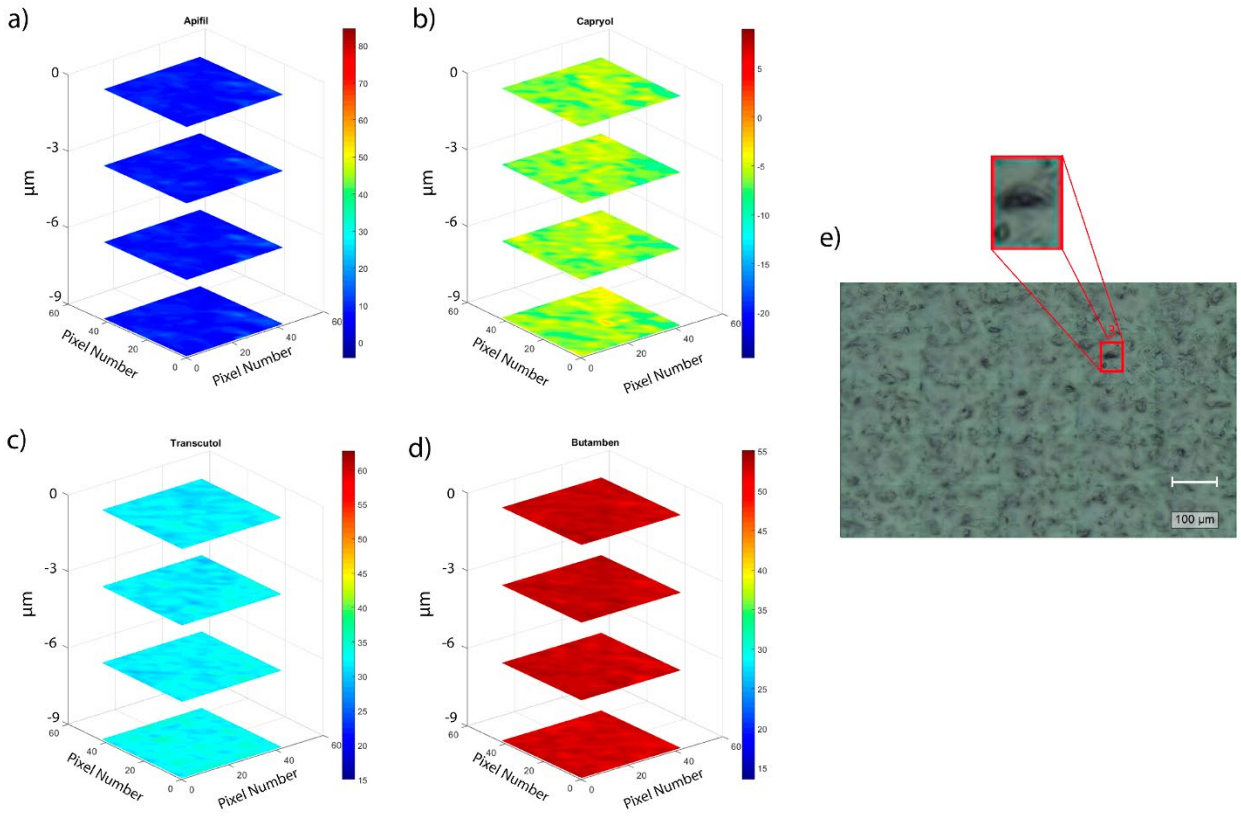

Figure 5. Volumetric Raman images obtained for a sample belongs to the homogeneous and smooth surface category (AM7) in the region 3 (red square in (e)) for: a) Apifil®, b) Capryol® 90, c) Transcutol® and d) BTB (Scale bar = 100µm, *x* axis = 560 µm, *y* axis = 860 µm).

In the smoother AM7 sample (Figure 5), the surface shows more solid lipid than in the internal layers, while liquid excipients are more concentrated in the deeper parts of the sample, i.e., below −6 µm. Similar observation was found for all samples where the concentration of liquid excipients, Capryol® 90 + Transcutol® is higher than 40% (w/w) (samples AM2, AM6, AM7, AM9, AM10, AM12, AM13 and AM15). In this sense, even if the excess of liquid excipients is expected to enhance miscibility of the API, here it induces phase separation. Similar behavior was found in all regions (Figures S7 to S10, Support Information).

Group 3 – Rough surfaces but homogeneous depth distribution.

Chemical maps from a representative region of sample AM4 are shown in Figure 6.

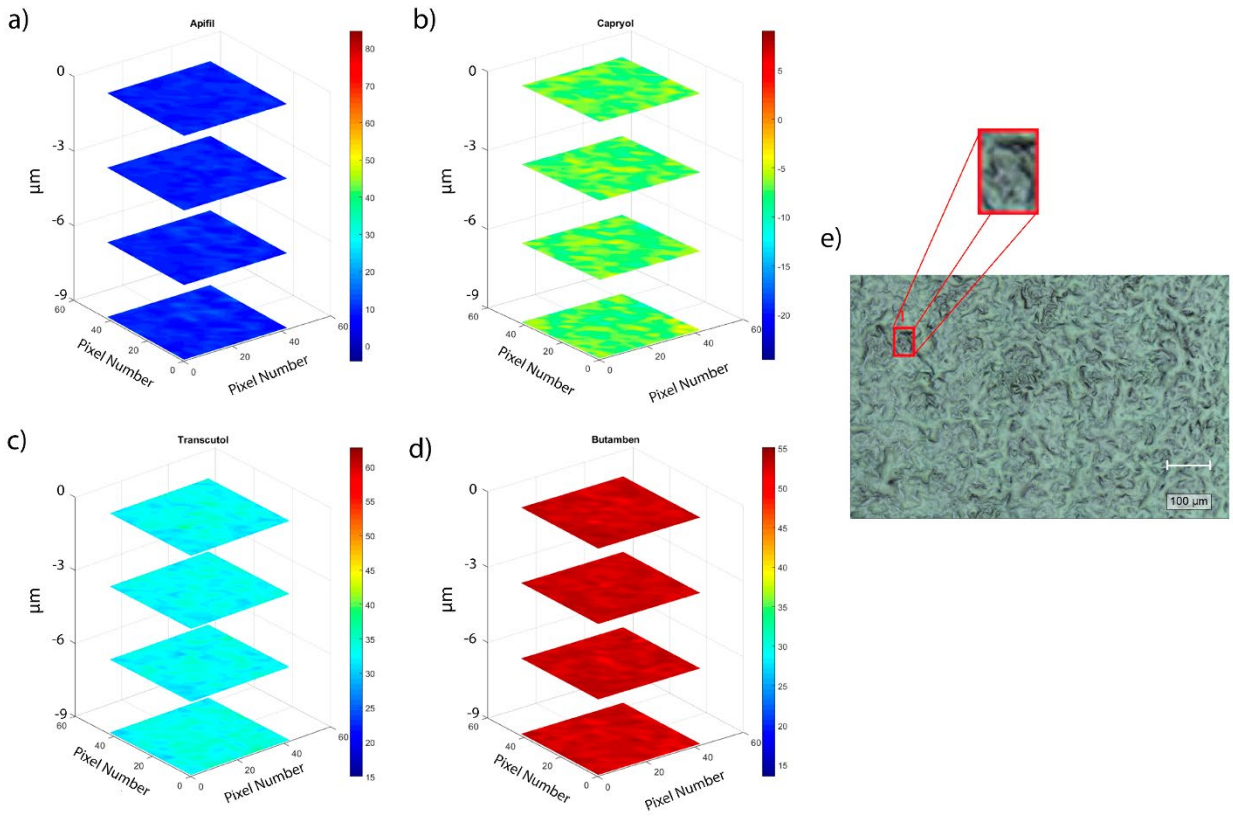

Figure 6. Volumetric Raman images obtained for a sample belongs to the homogeneous and rough surface category (AM4) in the region 4 (red square in (e)) for: a) Apifil®, b) Capryol® 90, c) Transcutol® and d) BTB (Scale bar = 100µm, *x* axis = 560 µm, *y* axis = 860 µm).

Differently from the other two groups, both surface and different layers were homogeneous. Thus, these samples show good miscibility without phase separation. In this classification, the amount of Transcutol® was below of 15% (w/w) and of Apifil® above 30% (w/w).

The importance of 3D imaging in the evaluation of miscibility is summarized in Table 2 and the main features are highlighted in italic. One important feature found in our samples is that a higher concentrations of Capryol® 90 and lower concentrations of Transcutol® provided better miscibility. However, if the concentration of Apifil® is low, phase separation occurs. Thus, a mixture DoE was used to find a good ratio between the excipients.

Table 2. Main conclusions obtained from Raman imaging in relation to confocal microscope image, chemical maps results and excipients concentrations, where the most important features are highlighted in italic.

Group	Visual Inspection and Samples	Chemical Inspection	Experimental Concentration
1	Heterogeneous (AM1, AM3, AM5, AM8, AM16)	Heterogeneous surface and in layers	*[Capryol® 90] = 10%(w/w)* 10% (w/w) < [Apifil®] < 40% (w/w) 10% (w/w) < [Transcutol®] < 40% (w/w) 20% (w/w) < [Transcutol® + Capryol® 90] < 50% (w/w)
2	Homogeneous and smooth (AM2, AM6, AM7, AM9, AM10, AM12AM13, AM15)	Surface homogeneous and heterogeneous in layers	15% (w/w) < [Capryol® 90] < 40%(w/w) *10% (w/w) < [Apifil®] < 20% (w/w)* 10% (w/w) < [Transcutol®] < 30% (w/w) *40% (w/w) < [Transcutol® + Capryol® 90] < 50% (w/w)*
3	Homogeneous and rough (AM4, AM11, AM14, AM17)	Homogeneous surface and layers	*10% (w/w) < [Capryol® 90] < 20%(w/w)* *30% (w/w) < [Apifil®] < 40% (w/w)* *10% (w/w) < [Transcutol®] < 15% (w/w)* 20% (w/w) < [Transcutol® + Capryol® 90] < 30% (w/w)

3.2. Mixture Design of Experiments

Table 3 shows input concentrations and the responses used in the mixture DoE.

Table 3. Standard deviation of maps (STD_{maps}) and Distributional Homogeneity Index (DHI) used as output parameters for the mixture DoE of the three groups of samples.

Sample Group		Apifil®		Capryol® 90		Transcutol®		BTB	
	Sample	STD_{maps}	DHI	STD_{maps}	DHI	STD_{maps}	DHI	STD_{maps}	DHI
1	AM1	8.36	2.89	1.39	2.1	4.23	4.07	2.37	3.61
	AM3	20.82	2.83	0.54	1.81	3.48	3.28	9.33	3.43
	AM5	10.1	3.67	0.91	2.55	1.77	4.64	3.13	3.78
	AM8	21.71	2.98	1.24	2.07	2.91	4.26	7.6	3.04
	AM16	15.58	2.93	0.94	1.93	1.57	3.85	4.77	3.51
2	AM2	0.24	1.65	0.18	1.35	0.25	2.7	0.07	2.47
	AM6	0.48	2.31	0.49	1.96	1.48	3.9	0.76	3.82
	AM7	0.27	2.25	0.22	2.06	0.44	4.43	0.24	4.1
	AM9	0.1	2.18	0.06	1.86	0.18	4.23	0.08	4.15
	AM10	16.55	2.18	0.64	1.92	0.54	3.74	6.59	3.16
	AM12	0.15	1.82	0.14	1.75	0.13	3.63	0.08	3.49
	AM13	0.33	1.92	0.2	1.84	0.09	3.81	0.04	3.66
	AM15	0.16	1.87	0.17	1.56	0.55	3.82	0.29	3.79
3	AM4	0.3	1.44	0.37	1.46	0.31	2.12	0.07	2.05
	AM11	11.61	2.36	0.89	1.71	1.65	2.84	3.81	2.47
	AM14	6.4	2.64	0.88	1.82	0.38	2.07	1.89	3.05
	AM17	2.31	1.93	1.13	1.59	0.54	3.81	0.47	3.74

Experimental design followed the lattice arrangement[23]. Sheffé models were built to describe the relationship between the concentrations and responses STD and DHI. Significant models were obtained for STD_{map} of Apifil®, Capryol® 90 and BTB, while DHI values were also significant for the lipids, i.e., Apifil® and Capryol® 90. The results are summarized in Table 4, from which we conclude that some responses, such as STD_{maps} and DHI of Apifil®, require more complex models other than linear ones. The significance level for ANOVA tests was 0.05.

Table 4. ANOVA summary of DoE results. The models were built using the lattice method in which the selection of composition points over all possible mixtures of components is obtained by analyzing the responses giving a uniform distribution of points.

Parameter	Model	Degrees of Freedom	p-value	Significant
STD_{map} – Apifil®	Special Quartic	8	0.0028	Yes
	Lack of Fit	4	0.0834	No
DHI – Apifil®	Cubic	9	0.0037	Yes
	Lack of Fit	3	0.3112	No
SDT_{map} – Capryol® 90	Linear	2	0.0018	Yes
	Lack of Fit	10	0.7998	No
DHI – Capryol® 90	Cubic	9	0.0277	Yes
	Lack of Fit	3	0.2869	No
STD_{map} - BTB	Linear	2	0.0020	Yes
	Lack of Fit	10	0.2964	No

An auxiliary way to evaluate the quality of the model is to analyze the behavior of the fit parameters and residuals, as shown for the DHI_{Apifil} (Figure 7). The normal plot of residuals (Figure 7a) indicates that residuals of the models follow a normal distribution, i.e., random behavior. Considering the randomness (Figures 7a and 7b), homoscedasticity (Figure 7b), and independency (Figure 7c) were observed, we can conclude that indeed the model describe the data well. Also, as the plot of predicted vs. actual values (Figure 7d) is satisfactory, the surface generated is suitable for our purposes. Similar outcomes were found for all other parameters (Figures S15 to S18).

Table 5 shows the values of the *b* coefficients, calculated by least squares linear regression and that described the surface/mathematical model, obtained for each term in mixture DoE for all significant inputs.

(i) Bold implies $p < 0.05$ and indicates the effect is very significant, while italic values indicate that p is between 0.05 and 0.1 and reflects an important effect.

(ii) Empty spaces denote that the coefficient is insignificant, $p > 0.1$.

(iii) Main effects, represented by a single letter in Table S1, were significant for the parameters studied.

(iv) Secondary and ternary effects, represented by more than one letter in Table 5, indicate that interactions between the excipients were important for all DHI values. On the other hand, for STD_{map} of Capryol® 90 and BTB maps these interactions were not significant.

Table 5. Coefficients obtained by mixture DoE model for each output. The statistical p-value is represented in *italic* if $p < 0.1$ and in **bold** if $p < 0.05$. Empty spaces mean not significant coefficients.

	A	B	C	AB	AC	BC	ABC	AB(A-B)	AC(A-C)	BC(B-C)	A^2BC	ABC^2
STD_{map} Apifil	**6.60**	**-0.45**	**19.61**								669.43	**-1299.23**
DHI Apifil	**2.75**	**1.75**	**2.86**		**2.26**		-13.34	**-5.55**	**5.53**			
STD_{map} Capryol	**1.11**	**0.03**	**0.67**									
DHI Capryol	**1.96**	**1.45**	**1.86**	0.06	**1.73**	1.01	-5.37	**-4.10**	2.33	0.0041		
STD_{map} BTB	**1.84**	**-0.82**	**6.60**									

A= Apifil®; B = Capryol® 90; C= Transcutol.

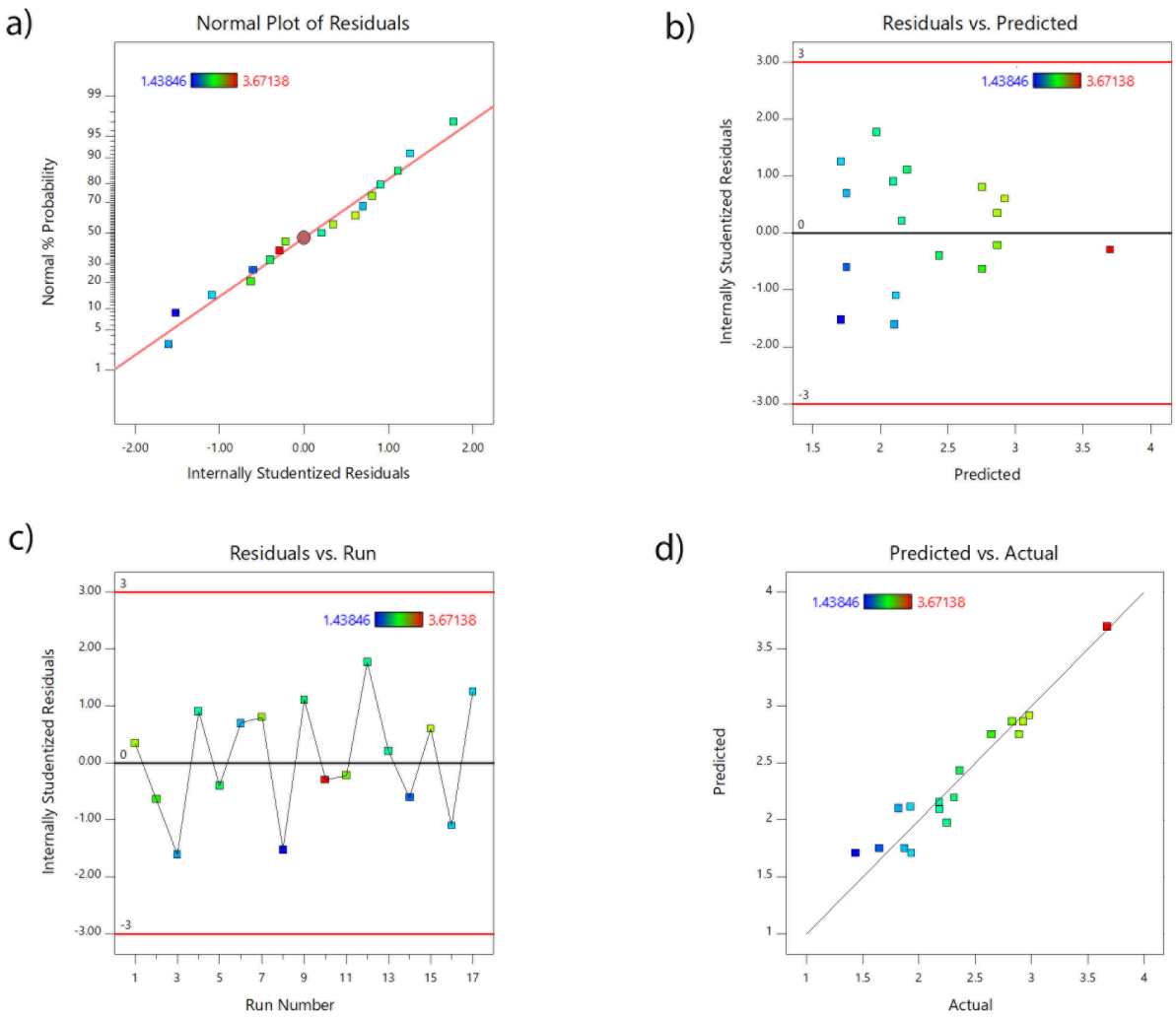

Figure 7. Diagnostic plots of DHI for Apifil: a) normal plot of residuals, b) internally studentized residuals *vs.* predicted values, c) internally studentized residuals *vs.* Run number and d) predicted values *vs.* Experimental values.

Figure 8 depicts the contour maps for each output showing the regions with higher homogeneity on the surface composition (lowest STD_{maps}) and the regions with similar layer composition (lowest DHI values). The main findings from this analysis were:

(i) for the excipients, higher concentration of Capryol® 90 and at least 20% (w/w) concentration of Apifil (blue part on Apifil® and Capryol® 90 STD_{map} surface, Figures 8a and 8c) are expected to give more homogeneous samples. Despite this, the highest value from BTB STD_{map}, red in this response surface, Figure 8e, shows a high concentration of Capryol® 90.

(ii) DHI was very affected by differences in layer composition, implying that analysis of this parameter can be used to avoid bad excipient proportions.

(iii) DHI response corroborates with our visible image description in which the region with highest heterogeneity corresponds to lower concentration of Capryol® 90. This happens because Capryol® 90 acts as a 'bridge' between Apifil® and Transcutol®, i.e., it has a good miscibility with both compounds.

(iv) Finally, regions with higher concentration of Transcutol® are more heterogeneous due to its hydrophilicity as seen in Figure 8.

Based on this outcome, an optimization step was followed to minimize DHI, STD_{map} and Transcutol® concentration and maximize Apifil® concentration to avoid phase separation. Two solutions were found:

- Solution 1: Apifil® 30.00% (w/w), Capryol 20.00% (w/w) and Transcutol 10.00% (w/w), with desirability of 0.783; and
- Solution 2: Apifil® 25.00% (w/w), Capryol 25.00% (w/w) and Transcutol 10.00% (w/w), with desirability of 0.742.

Sample AM4, which chemical maps are shown in Figure 6, has the same composition of Solution 1. It is striking that this sample had indeed the same aspect in all images without differences in composition between the layers, indicating the suitability of the approach followed here aiming to design clever experiments that will result in excipient homogeneity in preformulation stage.

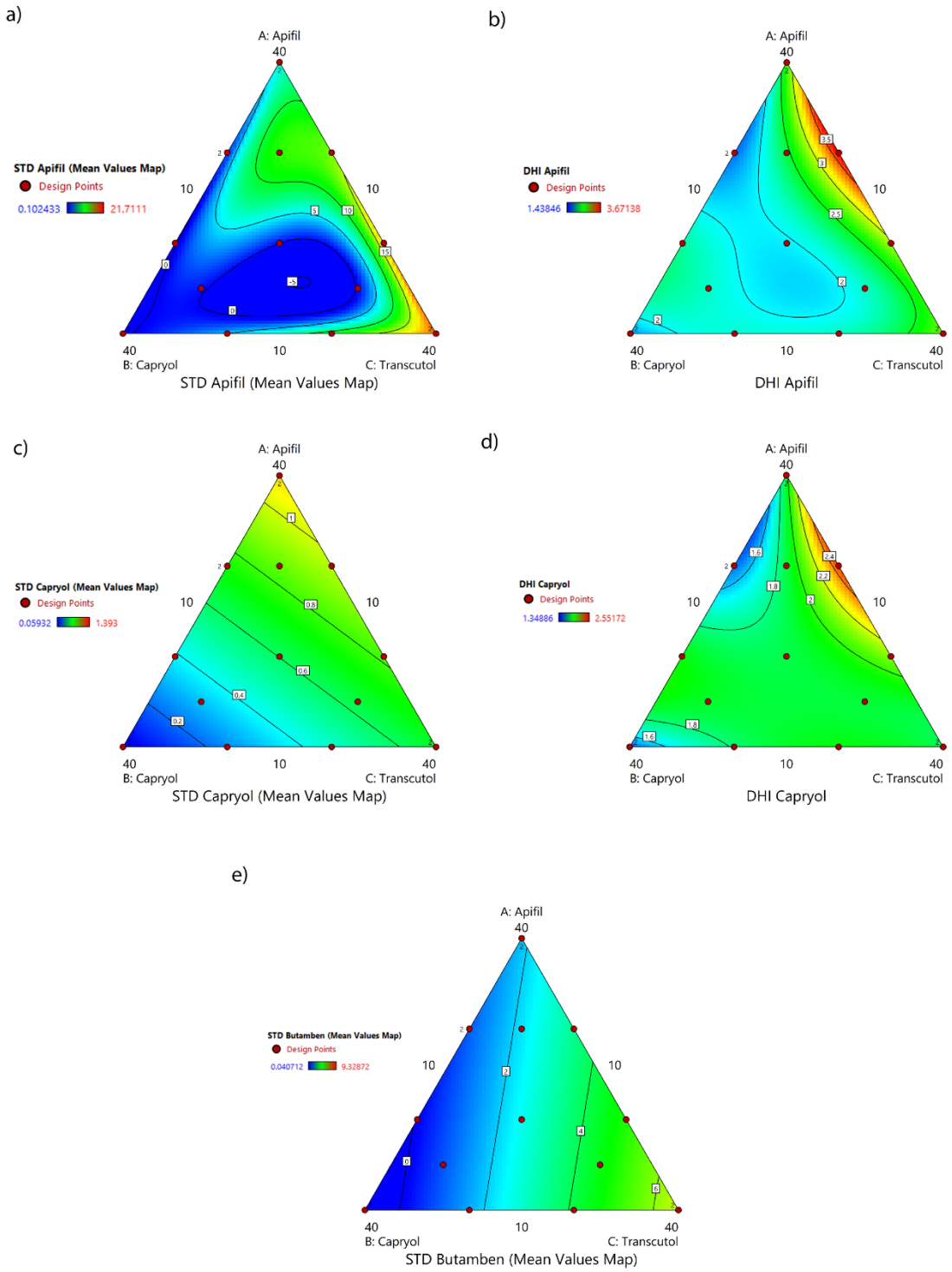

Figure 8. Contour maps for: a) DHI Apifil®, b) STD_{map} Apifil, c) DHI Capryol® 90, d) STD_{map} Capryol® 90 and e) STD_{map} BTB.

4. CONCLUSIONS

Confocal Raman microscopy combined with mixture DoE allowed predicting suitable formulations of the local anesthetic BTB for nanostructured lipid carriers. Homogeneity evaluation was visually analyzed in a random manner, to avoid bias, by means of microscopic image. From this procedure, the samples were grouped based on the different morphologies. Samples with the smallest Capryol® 90 concentration, that due its miscibility acts as a bridge with all compounds, showed very heterogenous surface (Group 1). Homogeneous and smooth surfaces were observed for those with concentration of liquid excipients higher than 40% (w/w) and Apifil® below of 20% (w/w) (Group 2). Finally, the third group, composed of samples with homogeneous and rough surfaces, had Capryol® 90 concentration ranging from 10.00 to 20.00% (w/w).

Following this step, 3D Raman imaging was used to differentiate the internal chemical distribution of Groups 2 and 3. Moreover, by combining Raman images with mixture DoE an overall view of the sample's behavior was obtained. From the output parameters, DHI and STD, and evaluation of the different compositions and surfaces, a distinction between excipient distribution in the layers was observed. This highlights the importance of excipients concentration in the sample homogeneity. A crucial observation was that even if higher concentration of liquid lipid, Capryol® 90, lead to a more homogeneous and smoother surface (Group 2), the samples showed different concentrations in the depth profiles. Finally, the model built using this methodology allowed to find that the sample with the highest desirability is a DoE point (sample AM4) – which belongs to group 3. Future steps of this research foresee the development of pharmaceutical formulations using this determined excipient proportions.

Declaration of Interest

The authors declare they have no conflict of interest.

AUTHOR INFORMATION

Corresponding Author

*Hery Mitsutake - herymitsutake@gmail.com

Author Contributions

The manuscript was written with the collaboration of all authors, who also approved the final version. **Hery Mitsutake:** methodology, investigation, formal analysis, software, writing – original draft; **Gustavo H. Rodrigues da Silva:** conceptualization**,** investigation, writing – review & editing; **Márcia C. Breitkreitz:** supervision (DoE), methodology, resources, project administration, writing – review & editing; **Eneida de Paula:** supervision (design of nanoparticles), methodology, resources, funding acquisition, project administration, writing – review & editing; **Heloisa N. Bordallo:** supervision (Raman imaging), methodology, resources, funding acquisition, project administration, writing – review & editing.

Funding Sources

São Paulo Research Foundation (FAPESP # 2018/22975-7 - H.M. and 2017/15174-5 – G.H.R.S. fellowships)

Conselho Nacional de Pesquisa (CNPq -E.P. fellowship)

CAPES (Code 001)

Niels Bohr Fund

Carlsberg Foundation (nº CF19-0521)

Instituto Nacional de Ciência e Tecnologia em Bioanalítica - INCTBio

ACKNOWLEDGMENT

The authors thank São Paulo Research Foundation (FAPESP # 2018/22975-7 - H.M. and 2017/15174-5 – G.H.R.S. fellowships), Conselho Nacional de Pesquisa (CNPq -E.P. fellowship), CAPES (Code 001), Carlsberg Foundation (nº CF19-0521) and Niels Bohr Fund for financial support. Also, the authors wish to thank Gattefossé (France) for the donation of excipients

ABBREVIATIONS

ANOVA, Analysis of variance; API, active pharmaceutical ingredient; BTB, butamben; CCD, charge-coupled device; CLS, classical least squares; DHI, distributional homogeneity index; DoE, design of experiments; LA, Local anesthetic; NIR, near infrared; STD_{maps}, standard deviation from mean values of each map.

REFERENCES

(1) de Araújo, D. R.; Ribeiro, L. N. de M.; de Paula, E. Lipid-Based Carriers for the Delivery of Local Anesthetics. *Expert Opin. Drug Deliv.* **2019**, *16* (7), 701–714. DOI:

10.1080/17425247.2019.1629415

(2) Harmatz, A. Local Anesthetics: Uses and Toxicities. *Surg. Clin. North Am.* **2009**, *89* (3), 587–598. DOI: 10.1016/j.suc.2009.03.008

(3) Rodrigues da Silva, G. H.; Lemes, J. B. P.; Geronimo, G.; de Lima, F. F.; de Moura, L. D.; dos Santos, A. C.; Carvalho, N. S.; Malange, K. F.; Breitkreitz, M. C.; Parada, C. A.; de Paula, E. Lipid Nanoparticles Loaded with Butamben and Designed to Improve Anesthesia at Inflamed Tissues. *Biomater. Sci.* **2021**, *9*, 3378–3389. DOI: 10.1039/d1bm00077b

(4) Cereda, C. M. S.; Guilherme, V. A.; Alkschbirs, M. I.; de Brito Junior, R. B.; Tofoli, G. R.; Franz-Montan, M.; de Araujo, D. R.; de Paula, E. Liposomal Butamben Gel Formulations: Toxicity Assays and Topical Anesthesia in an Animal Model. *J. Liposome Res.* **2017**, *27* (1), 74–82. DOI: 10.3109/08982104.2016.1160924

(5) Kovačević, A. B.; Müller, R. H.; Keck, C. M. Formulation Development of Lipid Nanoparticles: Improved Lipid Screening and Development of Tacrolimus Loaded Nanostructured Lipid Carriers (NLC). *Int. J. Pharm.* **2020**, *576*, 118918. DOI: 10.1016/j.ijpharm.2019.118918

(6) Mitsutake, H.; Rodrigues da Silva, G. H.; de Paula, E.; Breitkreitz, M. C. When It Is Too Much: Identifying Butamben Excess on the Surface of Pharmaceutical Preformulation Samples by Raman Mapping. Chemrxiv **2022**. DOI: 10.26434/chemrxiv-2022-5xrlm

(7) Breitkreitz, M. C.; Sabin, G. P.; Polla, G.; Poppi, R. J. Characterization of Semi-Solid Self-Emulsifying Drug Delivery Systems (SEDDS) of Atorvastatin Calcium by Raman Image Spectroscopy and Chemometrics. *J. Pharm. Biomed. Anal.* **2013**, *73*, 3–12. DOI:

10.1016/j.jpba.2012.03.054

(8) Beć, K. B.; Grabska, J.; Huck, C. W. Biomolecular and Bioanalytical Applications of Infrared Spectroscopy – A Review. *Anal. Chim. Acta* **2020**, *1133*, 150–177. DOI: 10.1016/j.aca.2020.04.015

(9) Ewing, A. V.; Kazarian, S. G. Recent Advances in the Applications of Vibrational Spectroscopic Imaging and Mapping to Pharmaceutical Formulations. *Spectrochim. Acta - Part A Mol. Biomol. Spectrosc.* **2018**, *197*, 10–29. DOI: 10.1016/j.saa.2017.12.055

(10) Sacré, P.-Y.; Lebrun, P.; Chavez, P.-F.; De Bleye, C.; Netchacovitch, L.; Rozet, E.; Klinkenberg, R.; Streel, B.; Hubert, P.; Ziemons, E. A New Criterion to Assess Distributional Homogeneity in Hyperspectral Images of Solid Pharmaceutical Dosage Forms. *Anal. Chim. Acta* **2014**, *818*, 7–14. DOI: 10.1016/j.aca.2014.02.014

(11) Farkas, A.; Nagy, B.; Marosi, G. Quantitative Evaluation of Drug Distribution in Tablets of Various Structures via Raman Mapping. *Period. Polytech. Chem. Eng.* **2018**, *62* (1), 1–7. DOI: 10.3311/PPch.10143

(12) Rocha de Oliveira, R.; de Juan, A. Design of Heterogeneity Indices for Blending Quality Assessment Based on Hyperspectral Images and Variographic Analysis. *Anal. Chem.* **2020**, *92* (24), 15880–15889. DOI: 10.1021/acs.analchem.0c03241

(13) Chavez, P.-F.; Lebrun, P.; Sacré, P.-Y.; De Bleye, C.; Netchacovitch, L.; Cuypers, S.; Mantanus, J.; Motte, H.; Schubert, M.; Evrard, B.; Hubert, P.; Ziemons, E. Optimization of a Pharmaceutical Tablet Formulation Based on a Design Space Approach and Using Vibrational Spectroscopy as PAT Tool. *Int. J. Pharm.* **2015**, *486* (1–2), 13–20. DOI:

10.1016/j.ijpharm.2015.03.025

(14) Rocha de Oliveira, R.; de Juan, A. SWiVIA – Sliding Window Variographic Image Analysis for Real-Time Assessment of Heterogeneity Indices in Blending Processes Monitored with Hyperspectral Imaging. *Anal. Chim. Acta* **2021**, *1180*, 338852. DOI: 10.1016/j.aca.2021.338852

(15) Ma, L.; Zhou, L.; Xu, M.; Huang, X.; Zhang, Q.; Dai, S.; Qiao, Y.; Wu, Z. Investigation of the Distributional Homogeneity on Chlorpheniramine Maleate Tablets Using NIR-CI. *Spectrochim. Acta - Part A Mol. Biomol. Spectrosc.* **2018**, *204*, 783–790. DOI: 10.1016/j.saa.2018.06.081

(16) Mitsutake, H.; Ribeiro, L. N. M.; Rodrigues da Silva, G. H.; Castro, S. R.; de Paula, E.; Poppi, R. J.; Breitkreitz, M. C. Evaluation of Miscibility and Polymorphism of Synthetic and Natural Lipids for Nanostructured Lipid Carrier (NLC) Formulations by Raman Mapping and Multivariate Curve Resolution (MCR). *Eur. J. Pharm. Sci.* **2019**, *135*, 51–59. DOI: 10.1016/j.ejps.2019.05.002

(17) Gotter, B.; Faubel, W.; Neubert, R. H. H. FTIR Microscopy and Confocal Raman Microscopy for Studying Lateral Drug Diffusion from a Semisolid Formulation. *Eur. J. Pharm. Biopharm.* **2010**, *74* (1), 14–20. DOI: 10.1016/j.ejpb.2009.07.006

(18) Chen, X.; Li, D.; Wang, H.; Jiao, Y.-Y; Wang, H.; Yu, Y.; Zhi, J. Fabrication of an EGF Modified Nanodiamonds-Based Anti-Cancer Drug Targeted Delivery System and Drug Carrier Uptake Visualization by 3D Raman Microscopy. *RSC Adv.* **2016**, *6* (50), 44543–44551. DOI: 10.1039/C6RA04753J

(19) Høgset, H.; Horgan, C. C.; Armstrong, J. P. K.; Bergholt, M. S.; Torraca, V.; Chen, Q.; Keane, T. J.; Bugeon, L.; Dallman, M. J.; Mostowy, S.; Stevens, M. M. In Vivo Biomolecular Imaging of Zebrafish Embryos Using Confocal Raman Spectroscopy. *Nat. Commun.* **2020**, *11* (1), 6172. DOI: 10.1038/s41467-020-19827-1

(20) Sabin, G. P.; de Souza, A. M.; Breitkreitz, M. C.; Poppi, R. J. Desenvolvimento de Um Algoritmo Para Identificação e Correção de Spikes Em Espectroscopia Raman de Imagem. *Quim. Nova* **2012**, *35* (3), 612–615. DOI: 10.1590/S0100-40422012000300030

(21) Ravn, C.; Skibsted, E.; Bro, R. Near-Infrared Chemical Imaging (NIR-CI) on Pharmaceutical Solid Dosage Forms—Comparing Common Calibration Approaches. *J. Pharm. Biomed. Anal.* **2008**, *48* (3), 554–561. DOI: 10.1016/j.jpba.2008.07.019

(22) Patnaik, P. Infrared and Raman Spectroscopy. In *Dean's Analytical Chemistry Handbook*; McGraw-Hill Education, 2004.

(23) Debrus, B.; Lebrun, P.; Ceccato, A.; Caliaro, G.; Rozet, E.; Nistor, I.; Oprean, R.; Rupérez, F. J.; Barbas, C.; Boulanger, B.; Hubert, P. Application of New Methodologies Based on Design of Experiments, Independent Component Analysis and Design Space for Robust Optimization in Liquid Chromatography. *Anal. Chim. Acta* **2011**, *691* (1–2), 33–42. DOI: 10.1016/j.aca.2011.02.035

Supporting Information

Neither too little nor too much: finding the ideal proportion of excipients

Hery Mitsutake[a,b*], Gustavo H. Rodrigues da Silva[a], Márcia C. Breitkreitz[c] , Eneida de Paula[a], Heloisa N. Bordallo[b]

[a] Department of Biochemistry and Tissue Biology, Institute of Biology, Unicamp, São Paulo, Brazil.

[b] Niels Bohr Institute, University of Copenhagen, Copenhagen, Denmark

[c] Department of Analytical Chemistry, Institute of Chemistry, University of Campinas (Unicamp), Campinas - São Paulo, Brazil.

AM3

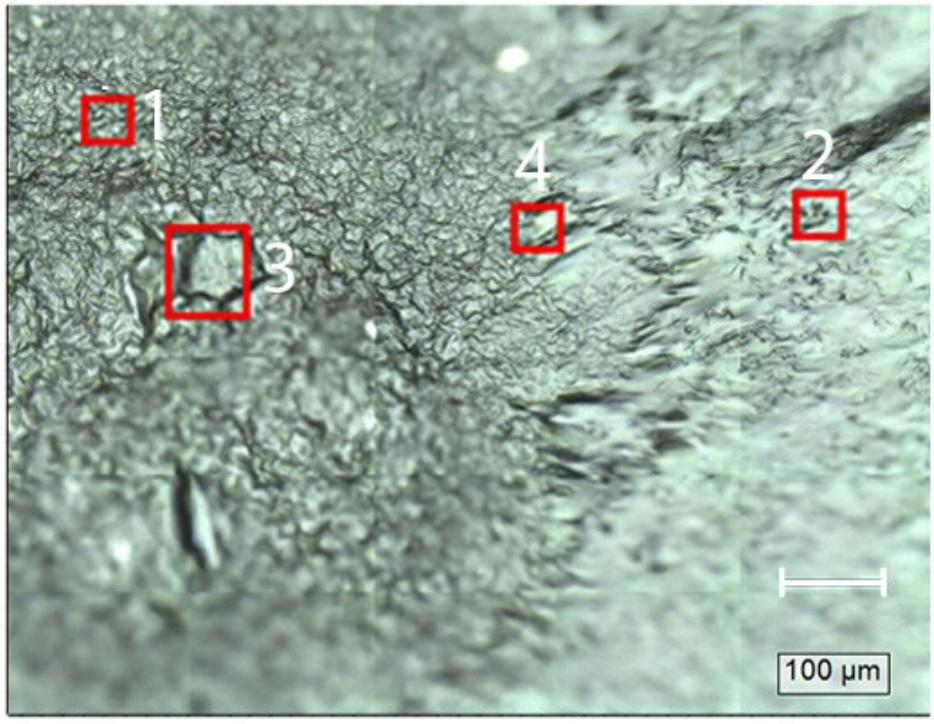

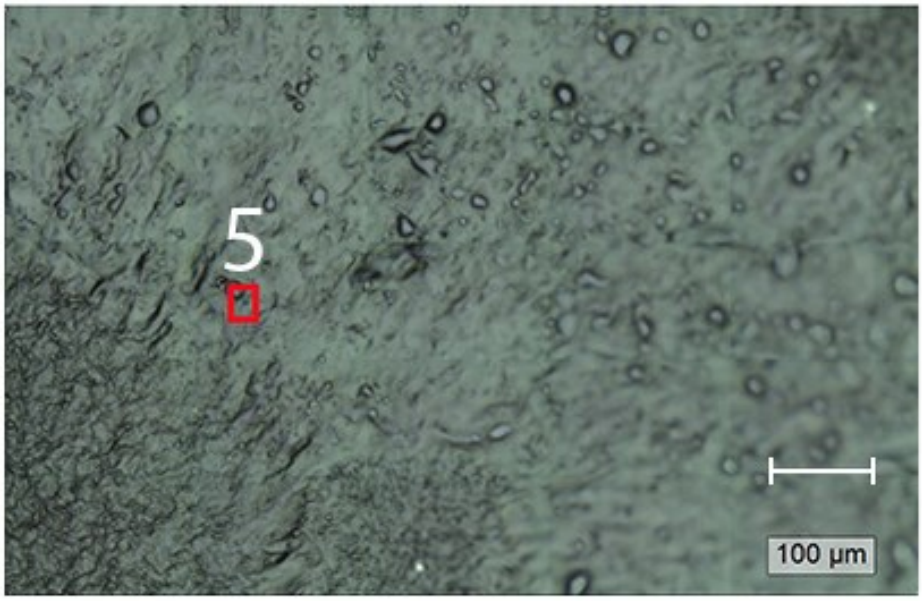

AM16

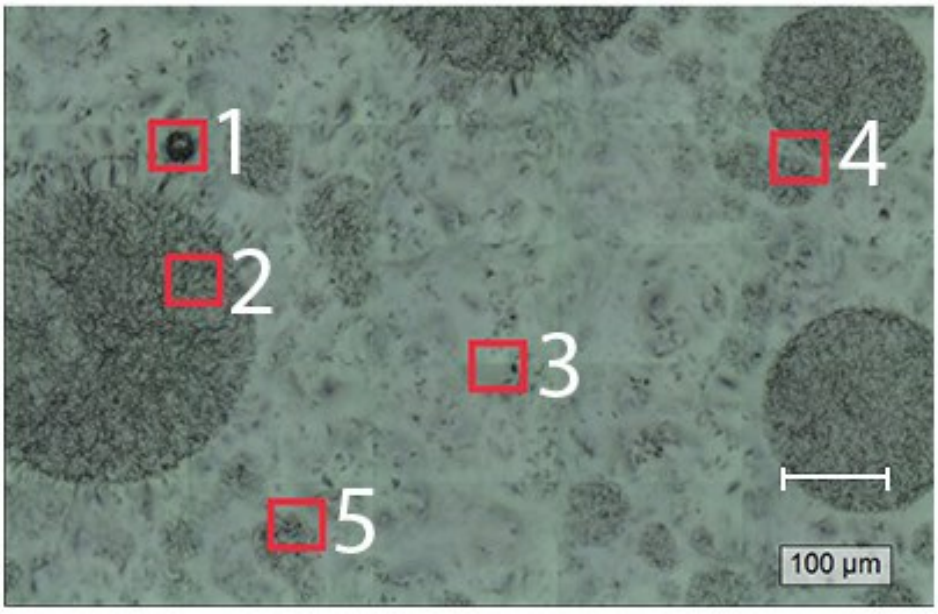

AM8

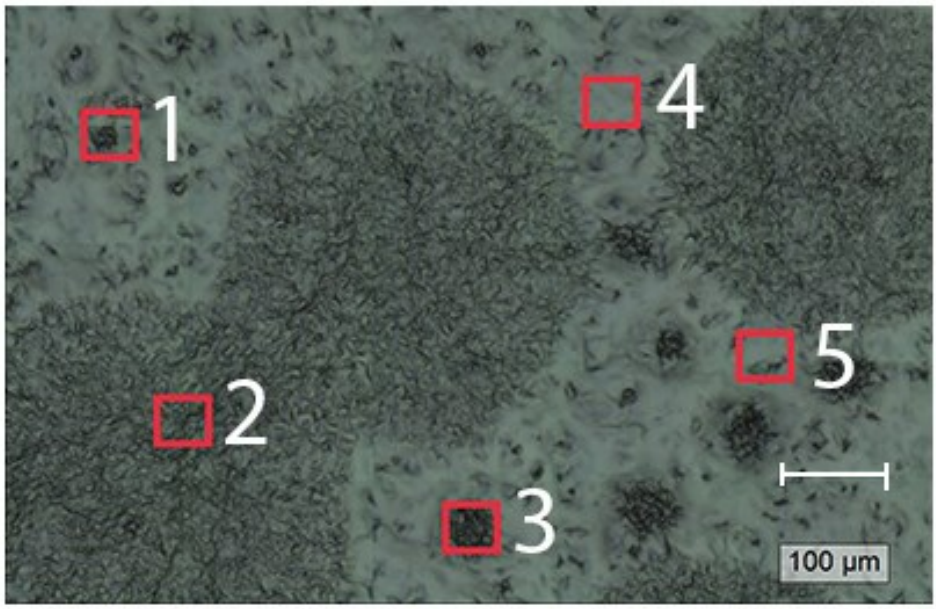

AM5

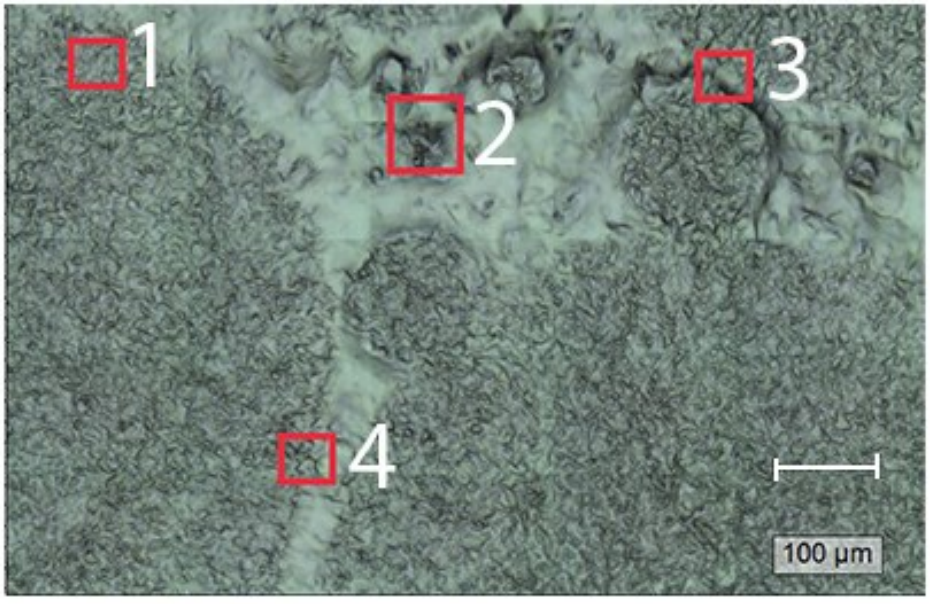

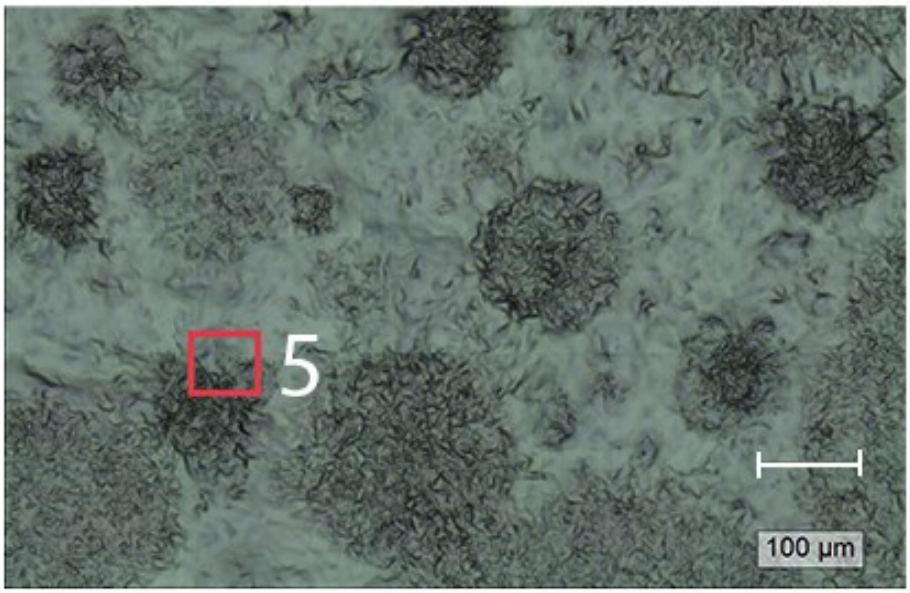

AM1

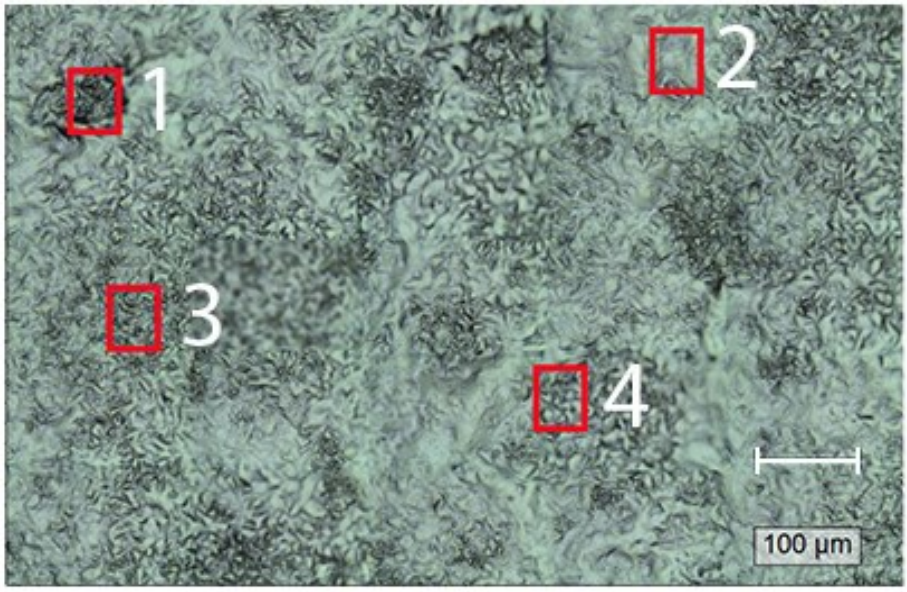

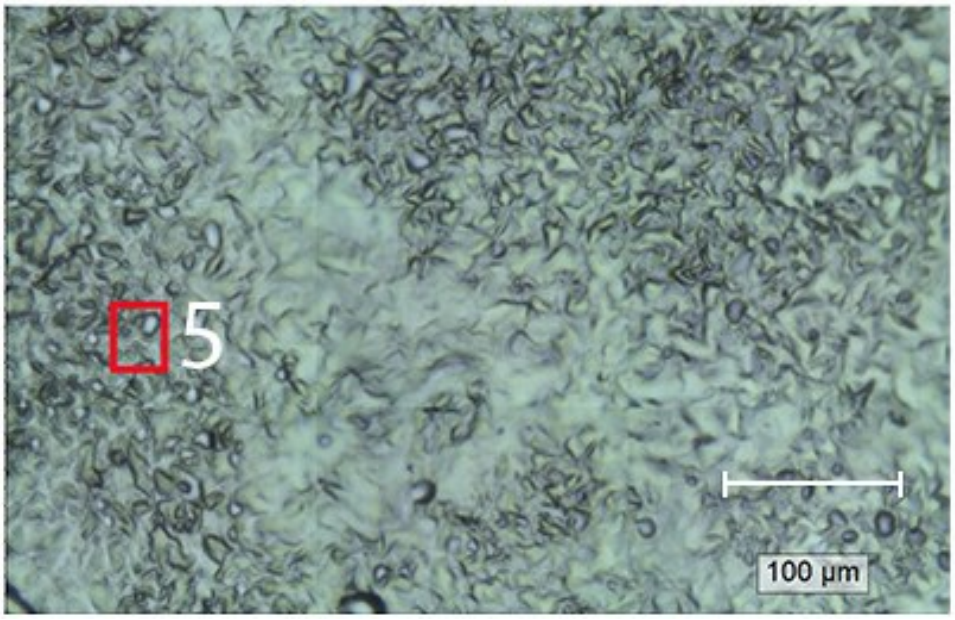

AM14

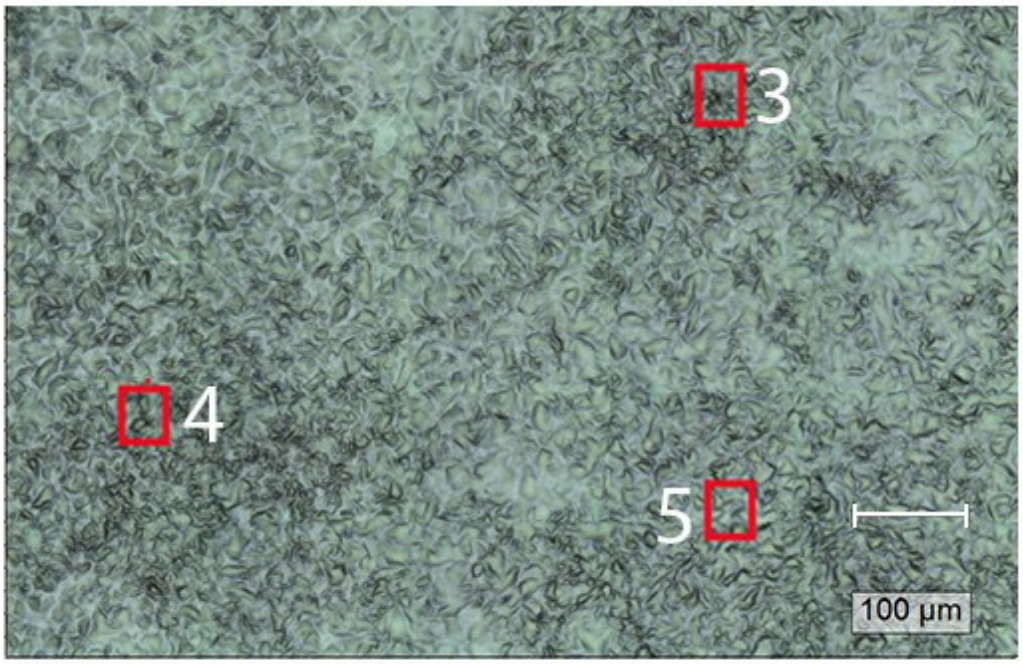

*regions 1 and 2 are acquired in other part of sample (not shown).

AM13

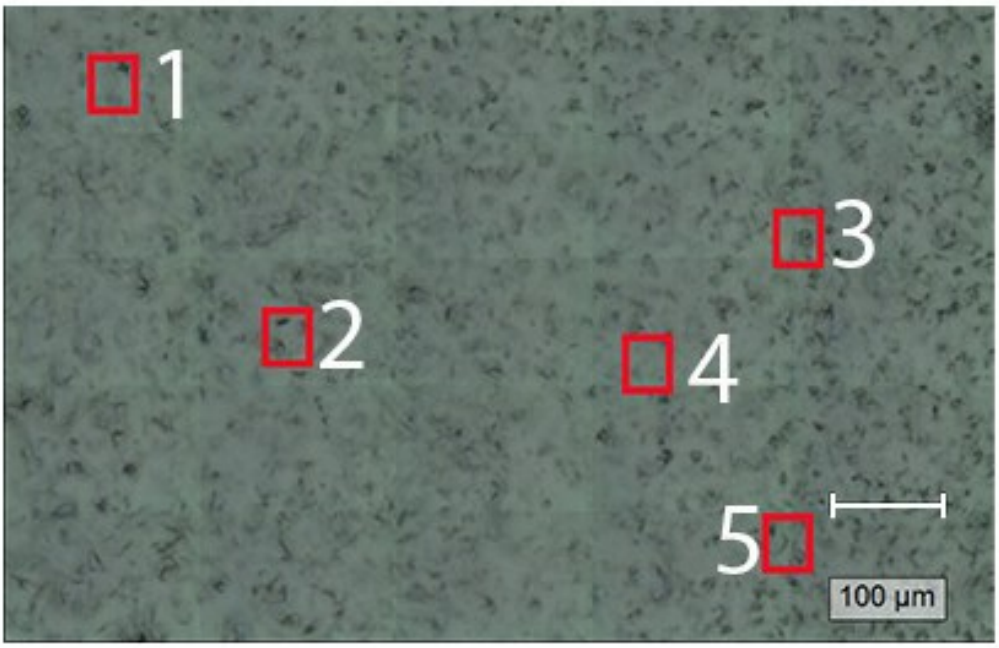

AM11

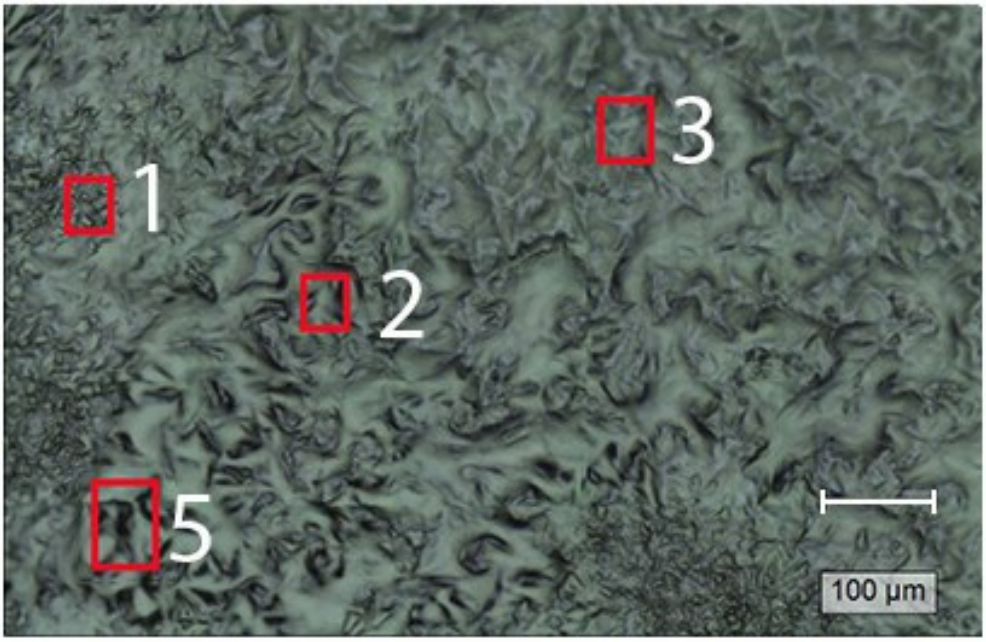

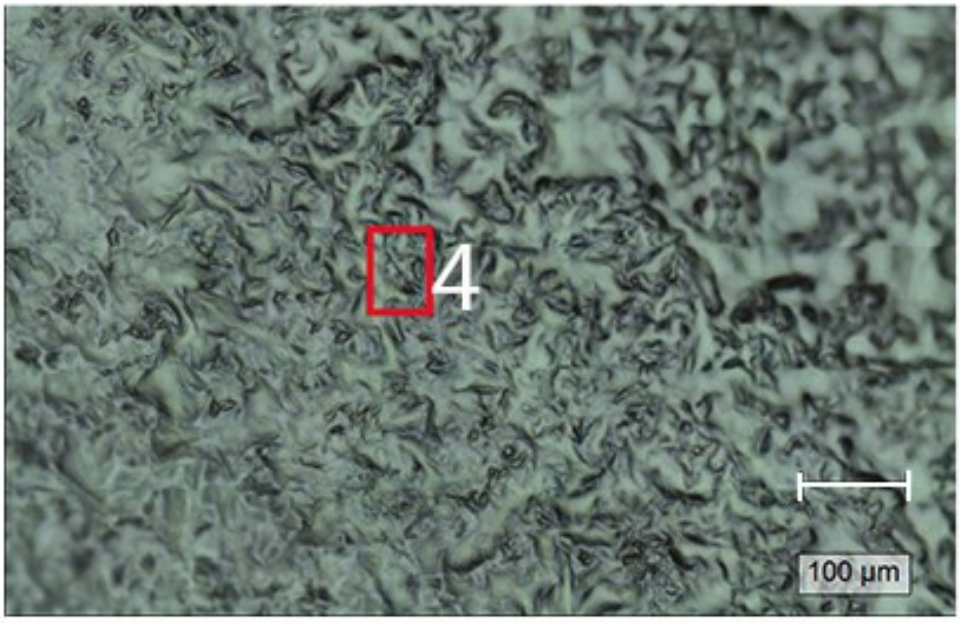

AM10

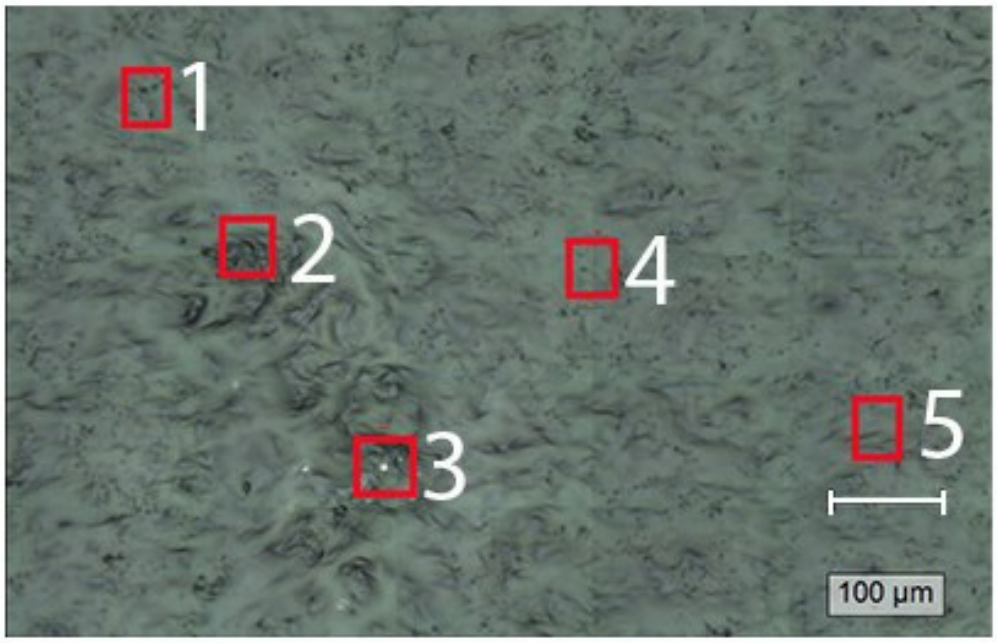

AM7

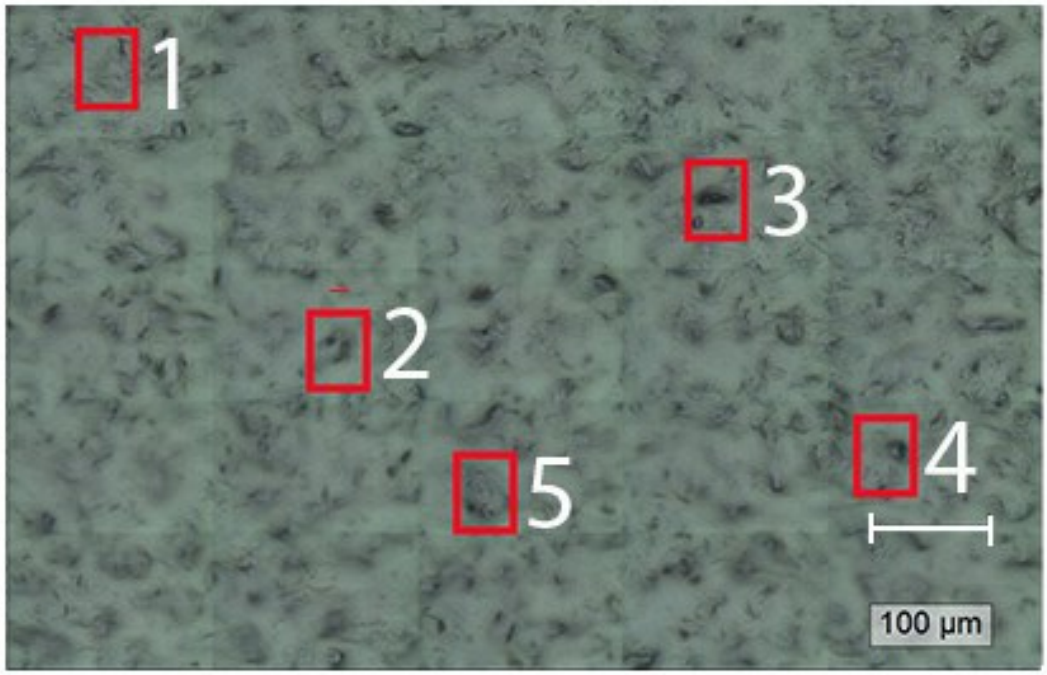

AM4

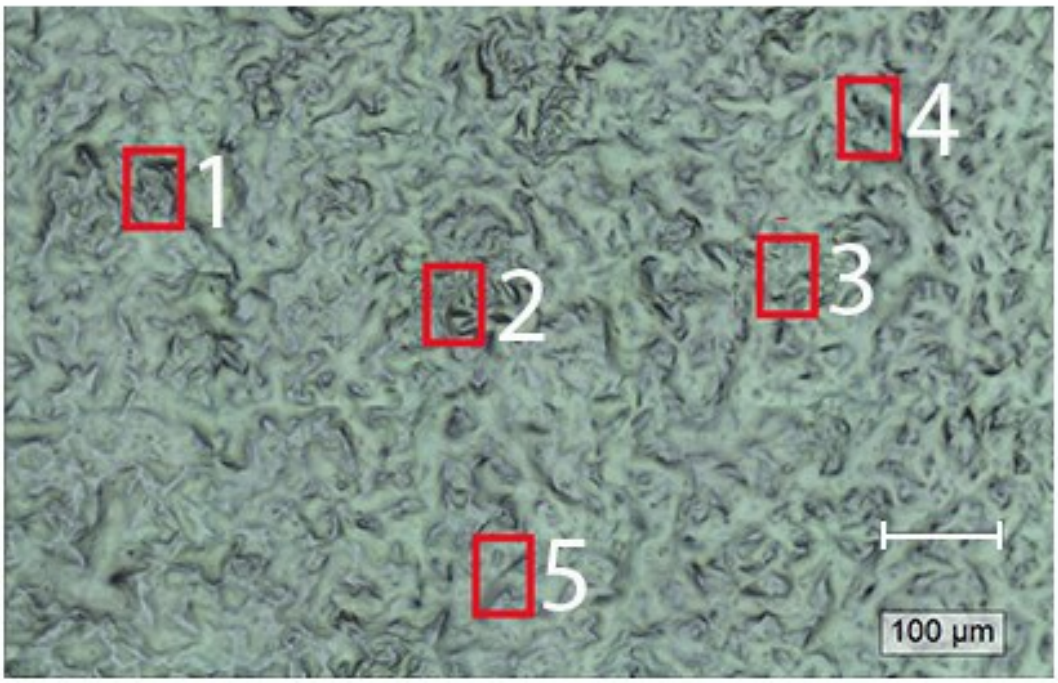

AM17

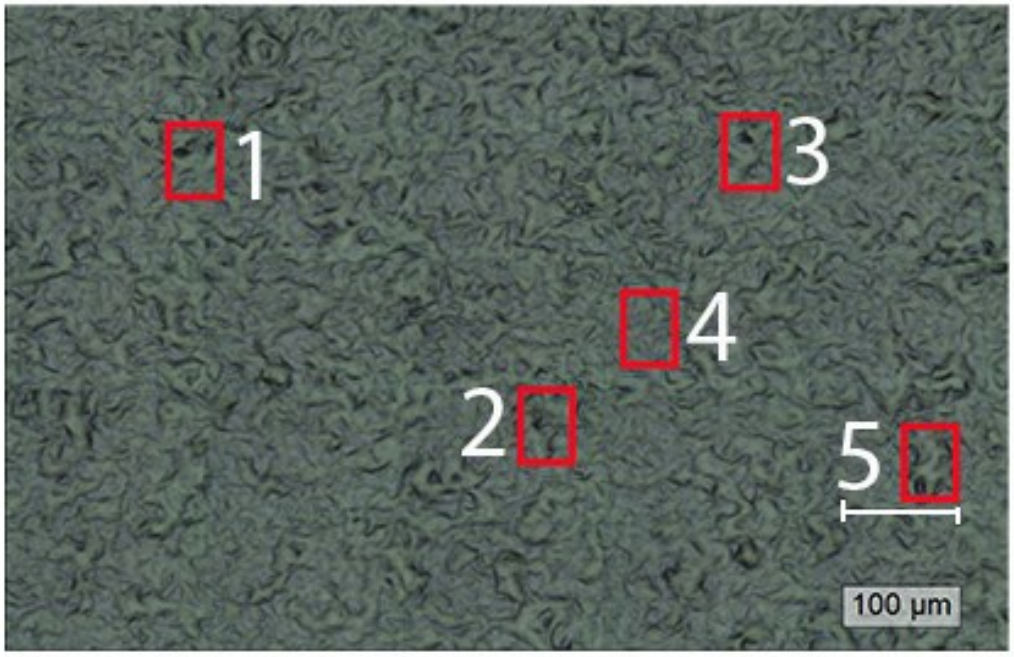

AM9

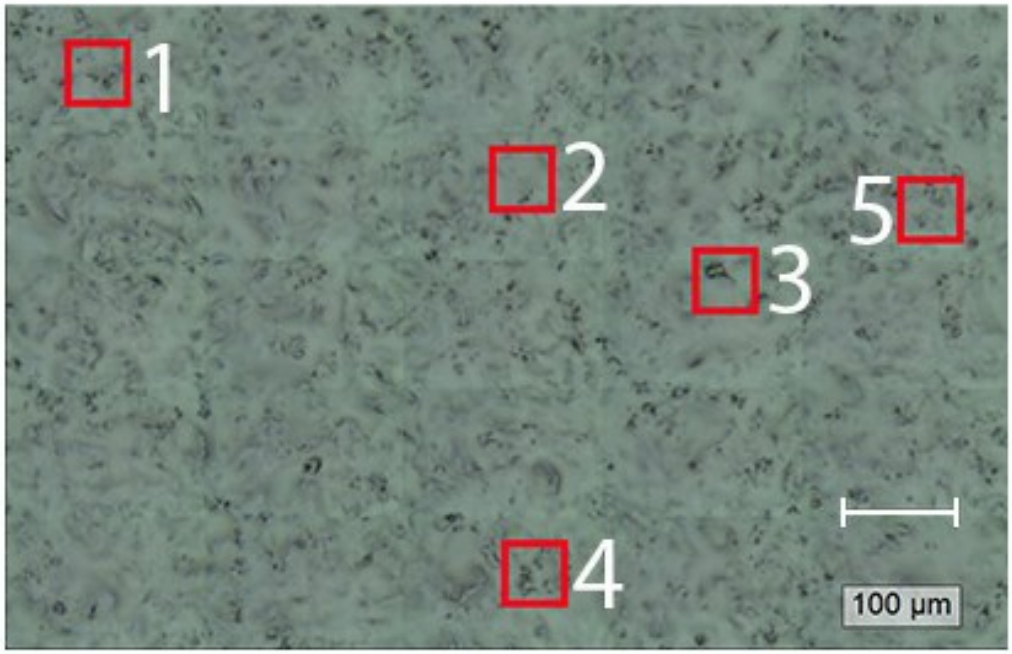

AM12

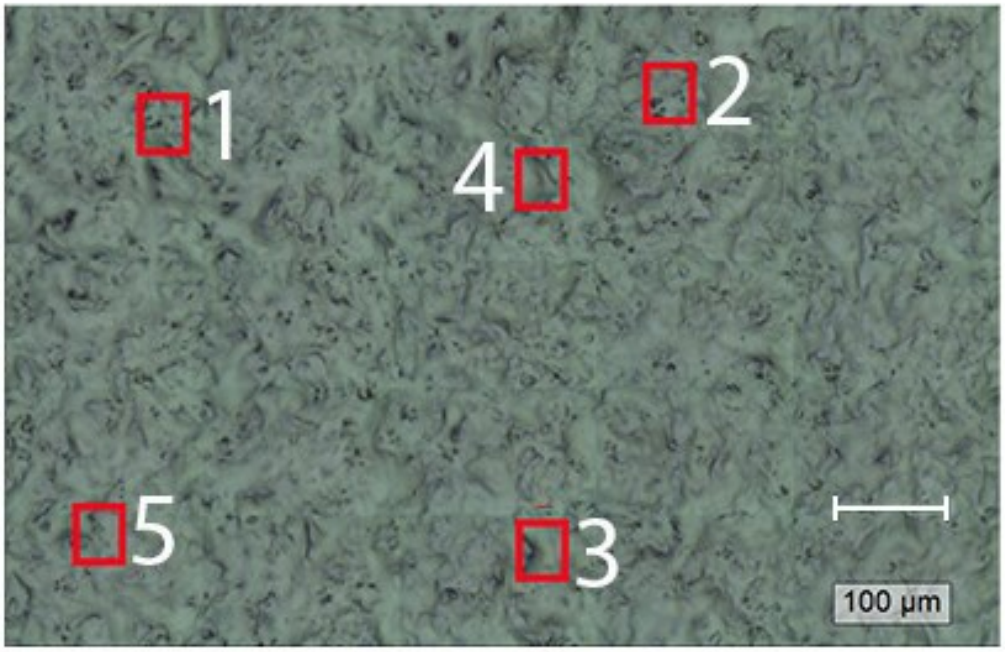

AM6

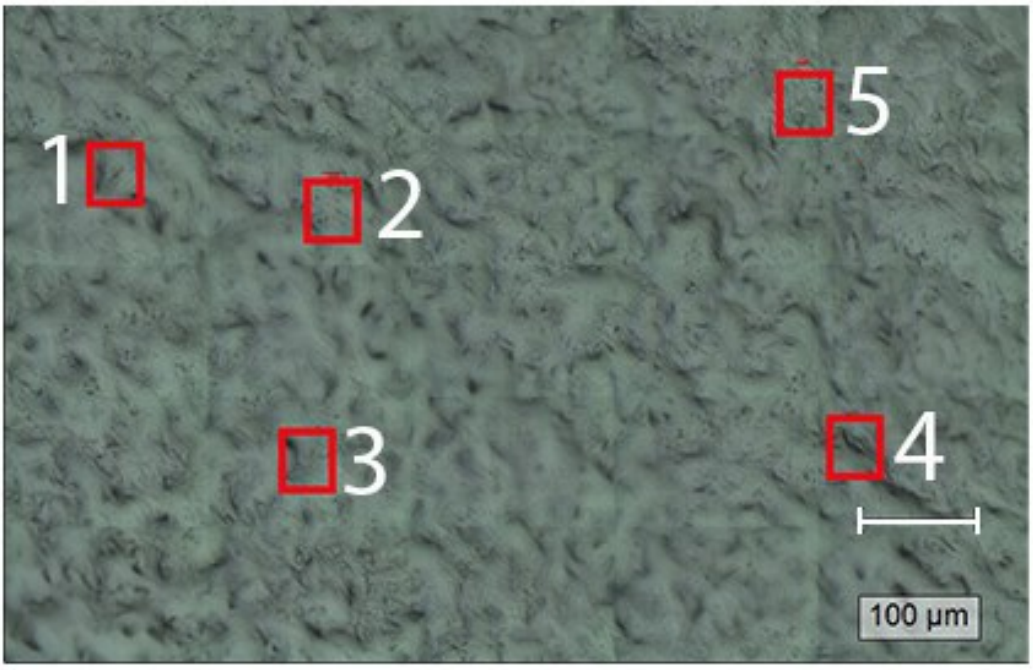

AM2

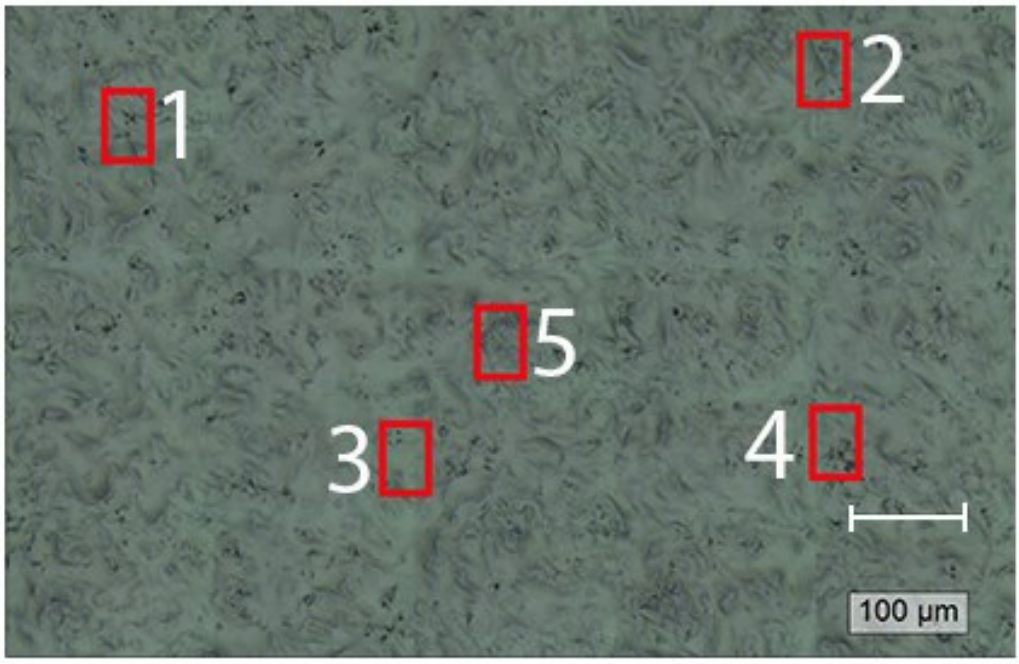

AM15

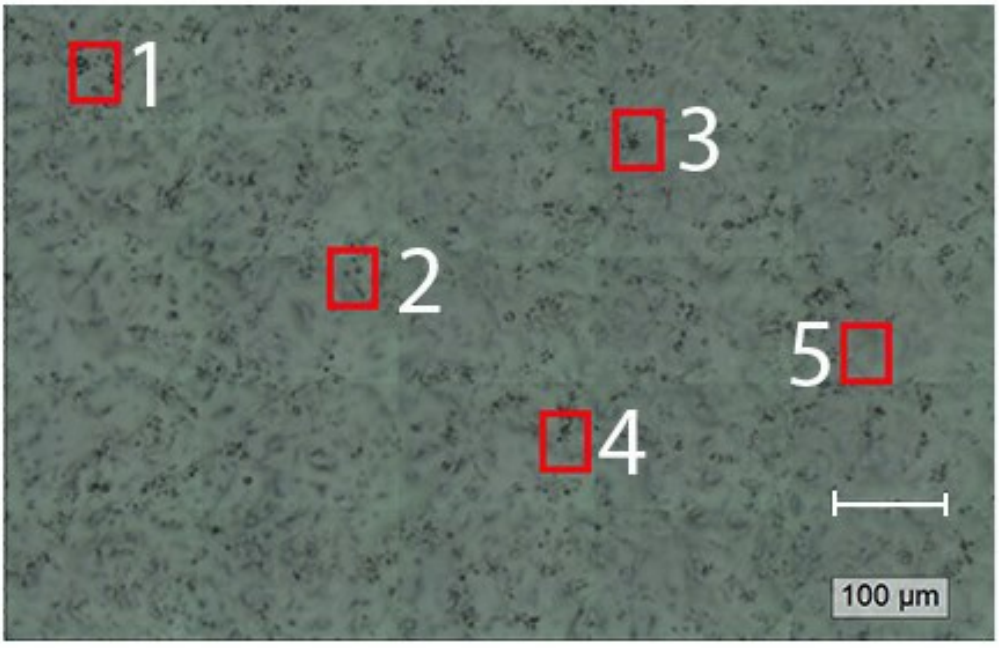

Figure S1. Confocal visible microscopic images of all samples used during Raman mapping. Red squares marked where the maps were made (Scale bar = 100µm, *x* axis = 560 µm, *y* axis = 860 µm).

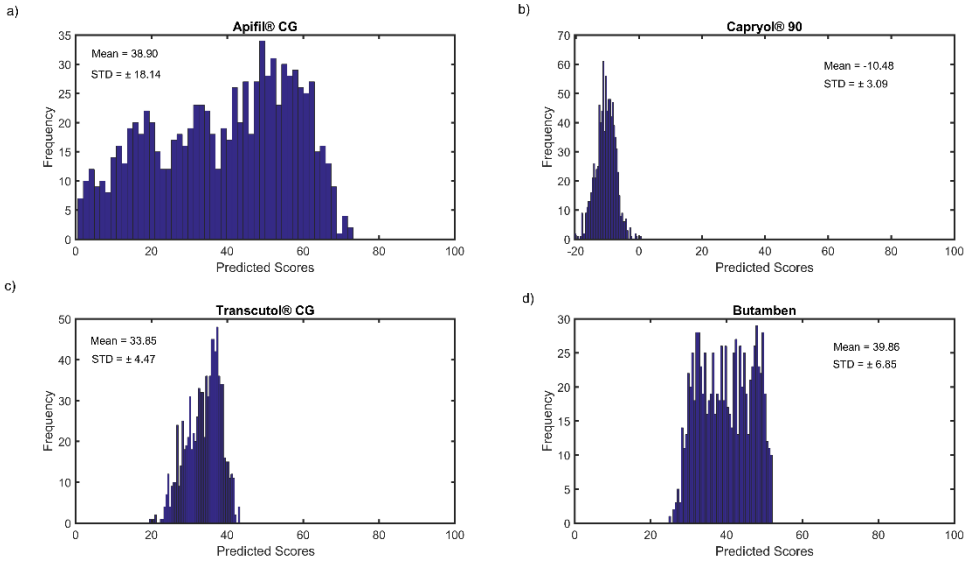

Figure S2. Histograms obtained by CLS model in sample AM8 for: a) Apifil® GC, b) Capryol® 90, c) Transcutol® GC and d) BTB.

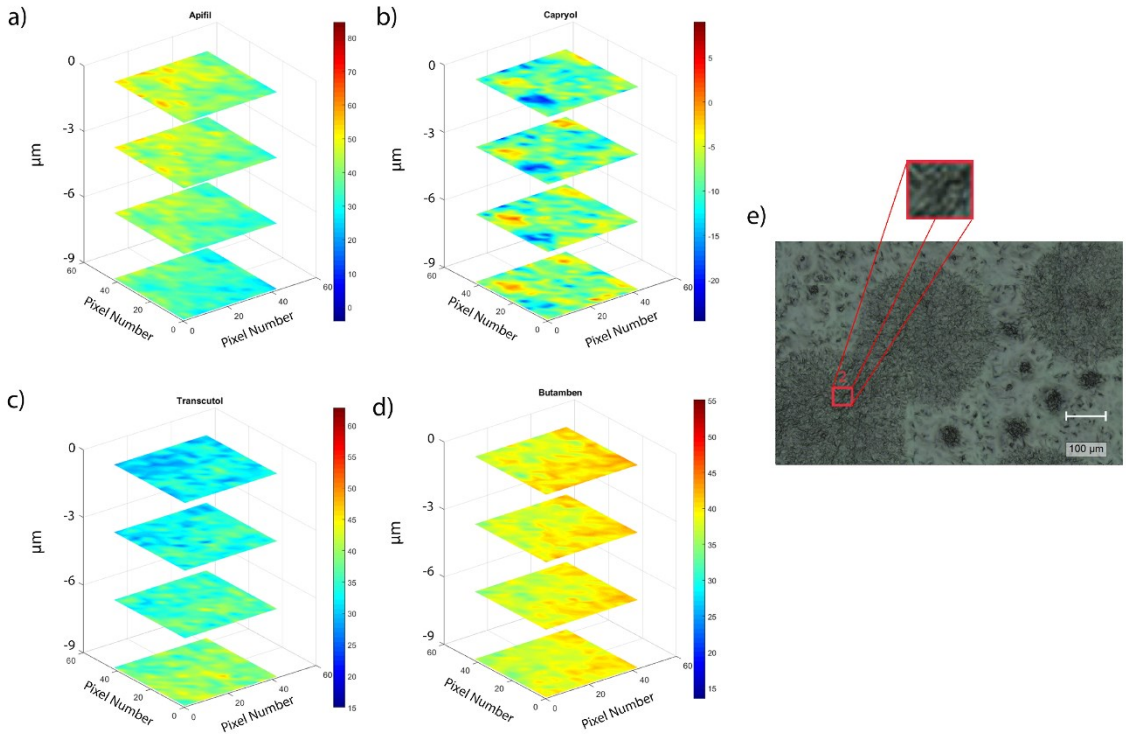

Figure S3. Volumetric Raman images obtained for a sample that belongs to the very heterogeneous category (AM8) in the region 2 (red square in (e)) for: a) Apifil®, b) Capryol® 90, c) Transcutol® and d) BTB (Scale bar = 100µm, *x* axis = 560 µm, *y* axis = 860 µm).

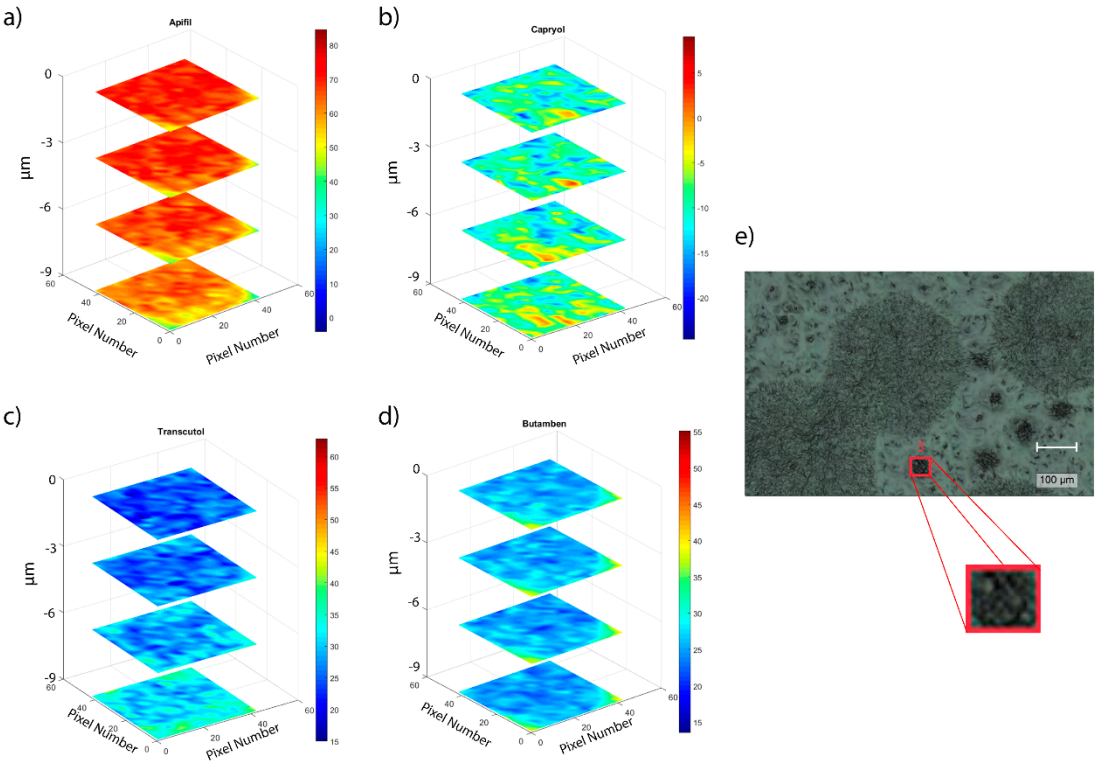

Figure S4. Volumetric Raman images obtained for a sample belongs to the very heterogeneous category (AM8) in the region 3 (red square in (e)) for: a) Apifil®, b) Capryol® 90, c) Transcutol® and d) BTB (Scale bar = 100µm, *x* axis = 560 µm, *y* axis = 860 µm).

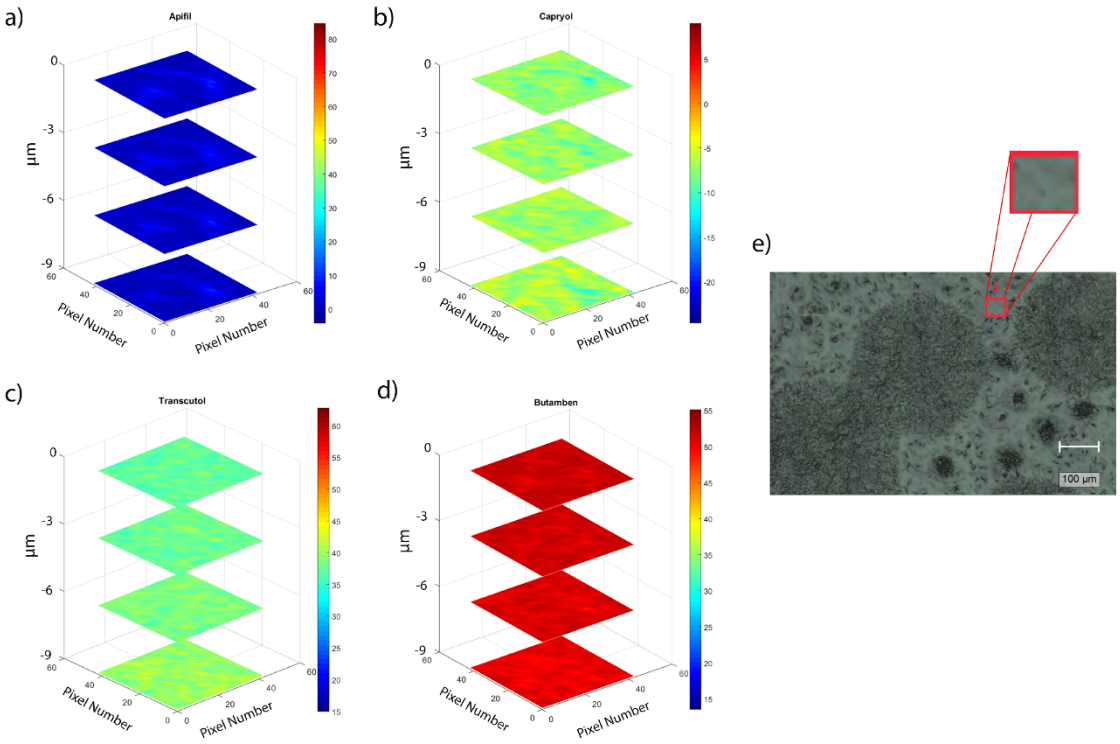

Figure S5. Volumetric Raman images obtained for a sample belongs to the very heterogeneous category (AM8) in the region 4 (red square in (e)) for: a) Apifil®, b) Capryol® 90, c) Transcutol® and d) BTB (Scale bar = 100µm, *x* axis = 560 µm, *y* axis = 860 µm).

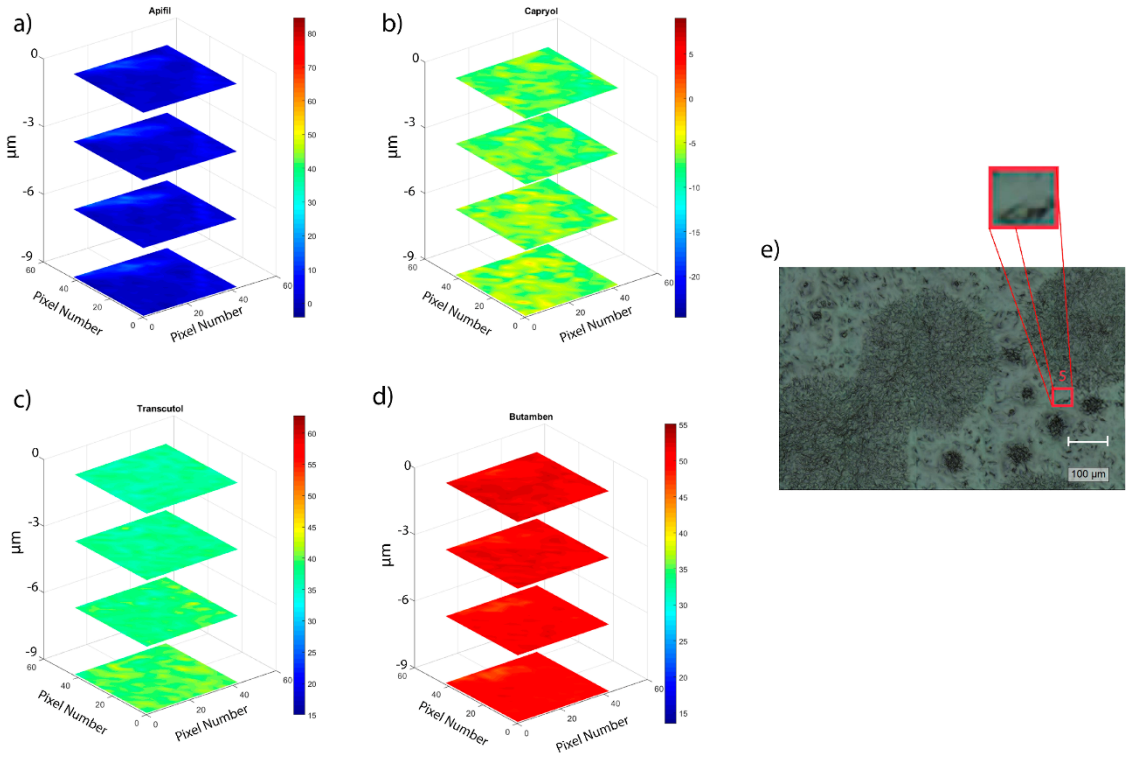

Figure S6. Volumetric Raman images obtained for a sample belongs to the very heterogeneous category (AM8) in the region 5 (red square in (e)) for: a) Apifil®, b) Capryol® 90, c) Transcutol® and d) BTB (Scale bar = 100µm, *x* axis = 560 µm, *y* axis = 860 µm).

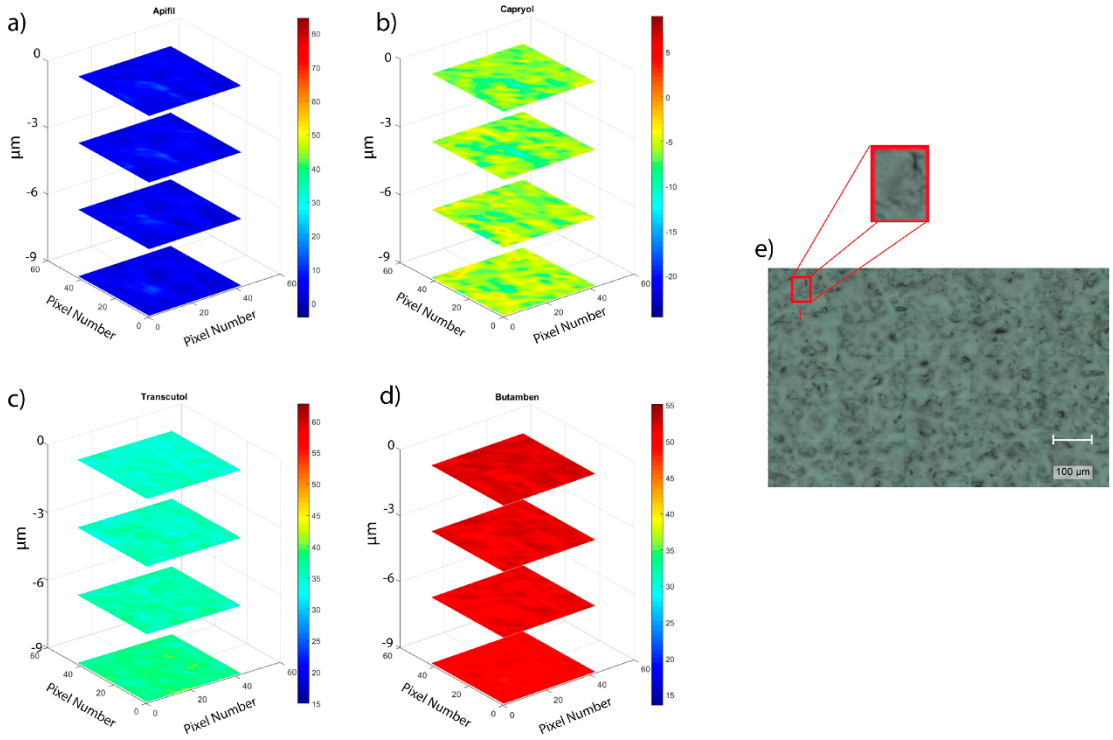

Figure S7. Volumetric Raman images obtained for a sample belongs to the homogeneous and smooth surface category (AM7) in the region 1 (red square in (e)) for: a) Apifil®, b) Capryol® 90, c) Transcutol® and d) BTB (Scale bar = 100µm, *x* axis = 560 µm, *y* axis = 860 µm).

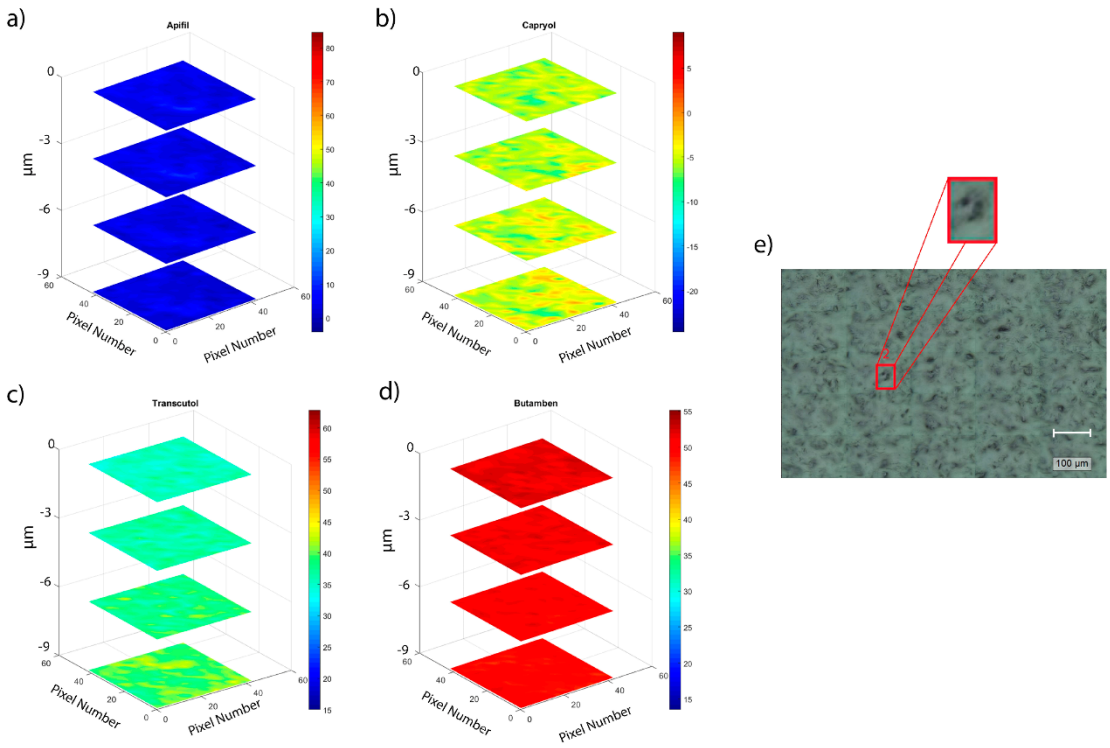

Figure S8. Volumetric Raman images obtained for a sample belongs to the homogeneous and smooth surface category (AM7) in the region 2 (red square in (e)) for: a) Apifil®, b) Capryol® 90, c) Transcutol® and d) BTB (Scale bar = 100µm, *x* axis = 560 µm, *y* axis = 860 µm).

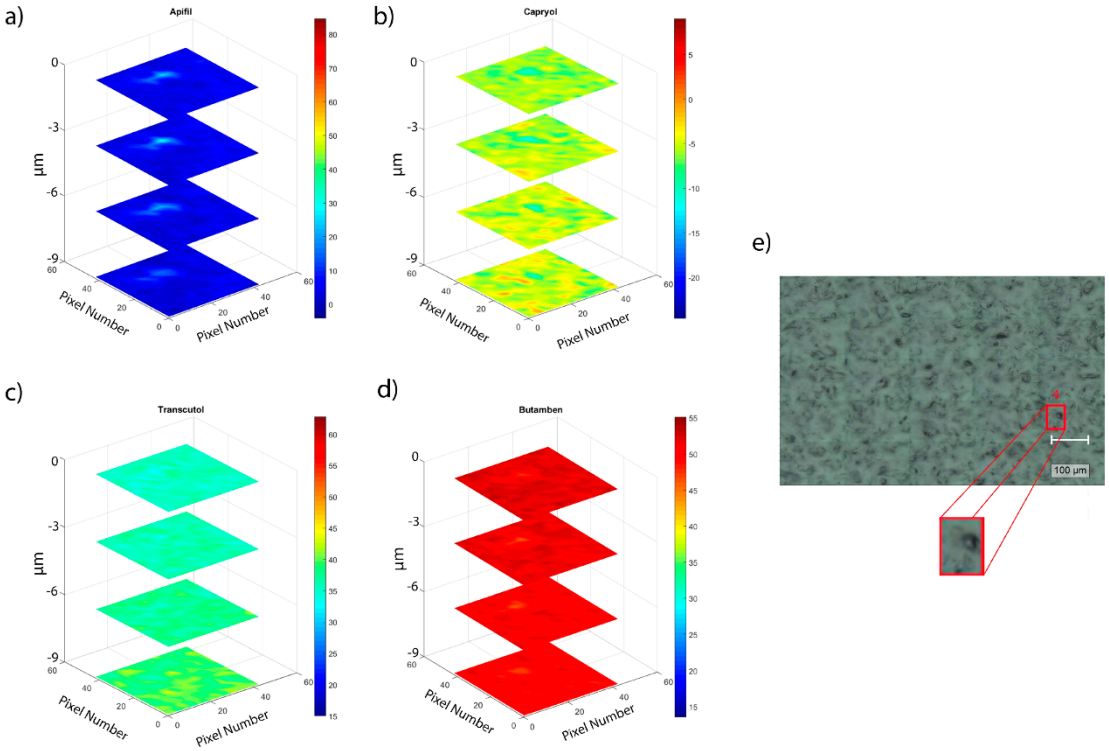

Figure S9. Volumetric Raman images obtained for a sample belongs to the homogeneous and smooth surface category (AM7) in the region 4 (red square in (e)) for: a) Apifil®, b) Capryol® 90, c) Transcutol® and d) BTB (Scale bar = 100µm, *x* axis = 560 µm, *y* axis = 860 µm).

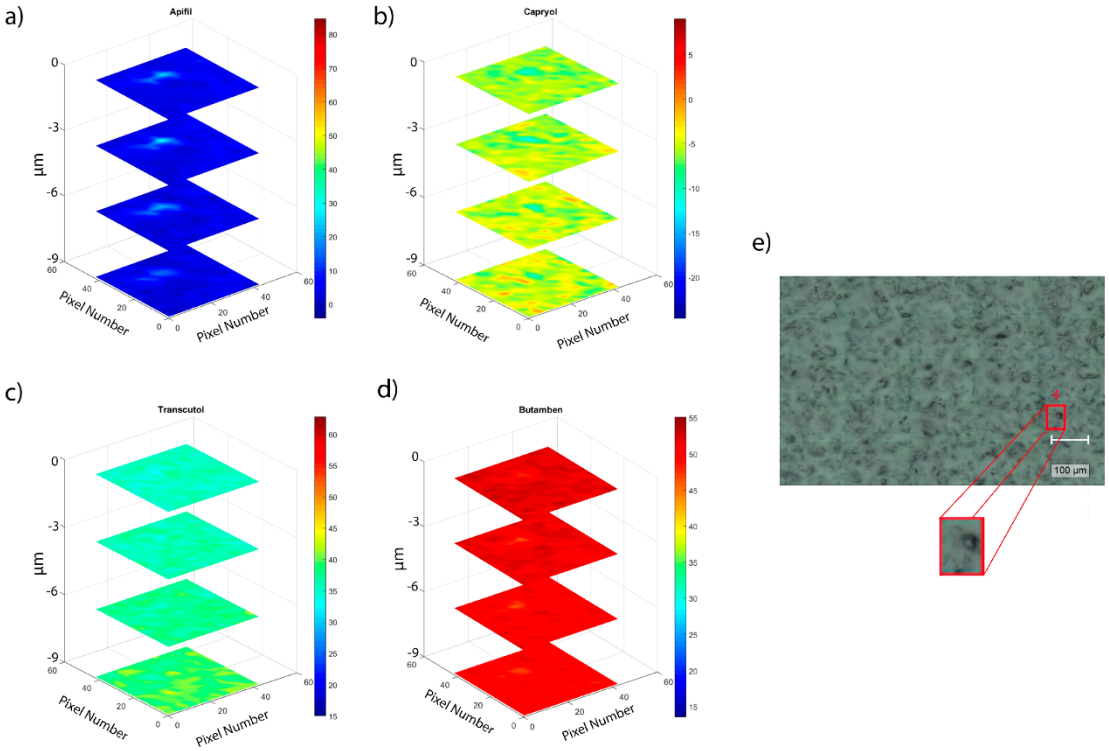

Figure S10. Volumetric Raman images obtained for a sample belongs to the homogeneous and smooth surface category (AM7) in the region 5 (red square in (e)) for: a) Apifil®, b) Capryol® 90, c) Transcutol® and d) BTB (Scale bar = 100µm, *x* axis = 560 µm, *y* axis = 860 µm).

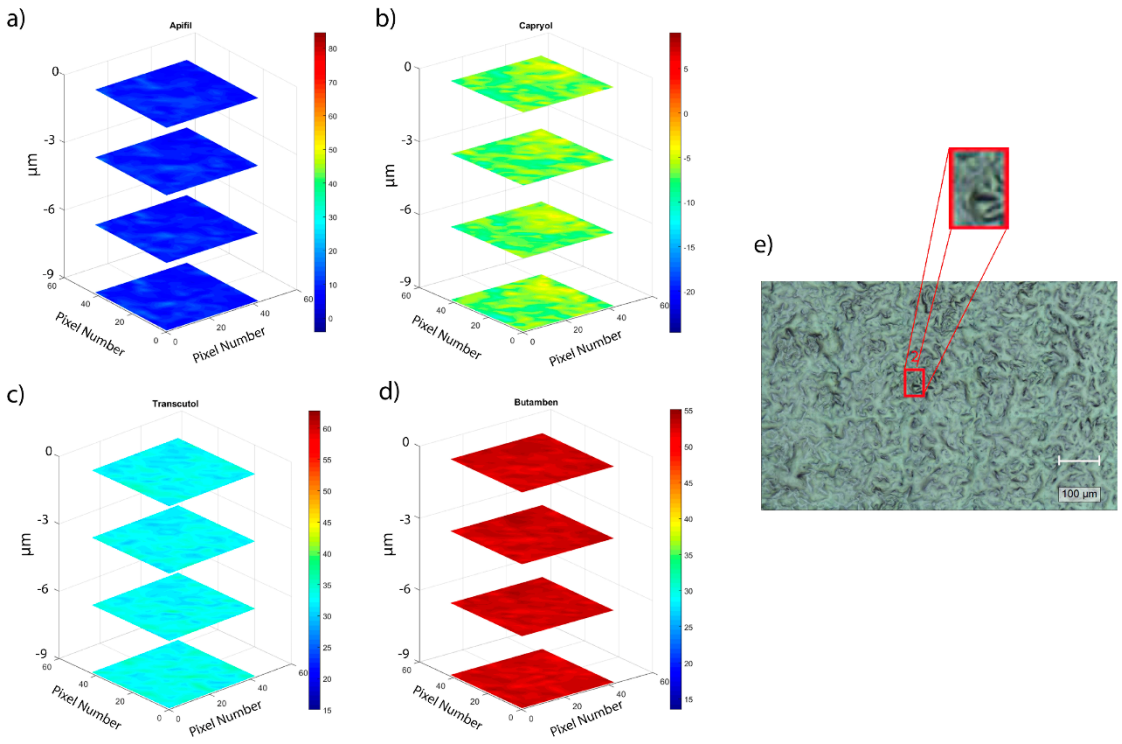

Figure S11. Volumetric Raman images obtained for a sample belongs to the homogeneous and rough surface category (AM4) in the region 2 (red square in (e)) for: a) Apifil®, b) Capryol® 90, c) Transcutol® and d) BTB (Scale bar = 100µm, *x* axis = 560 µm, *y* axis = 860 µm).

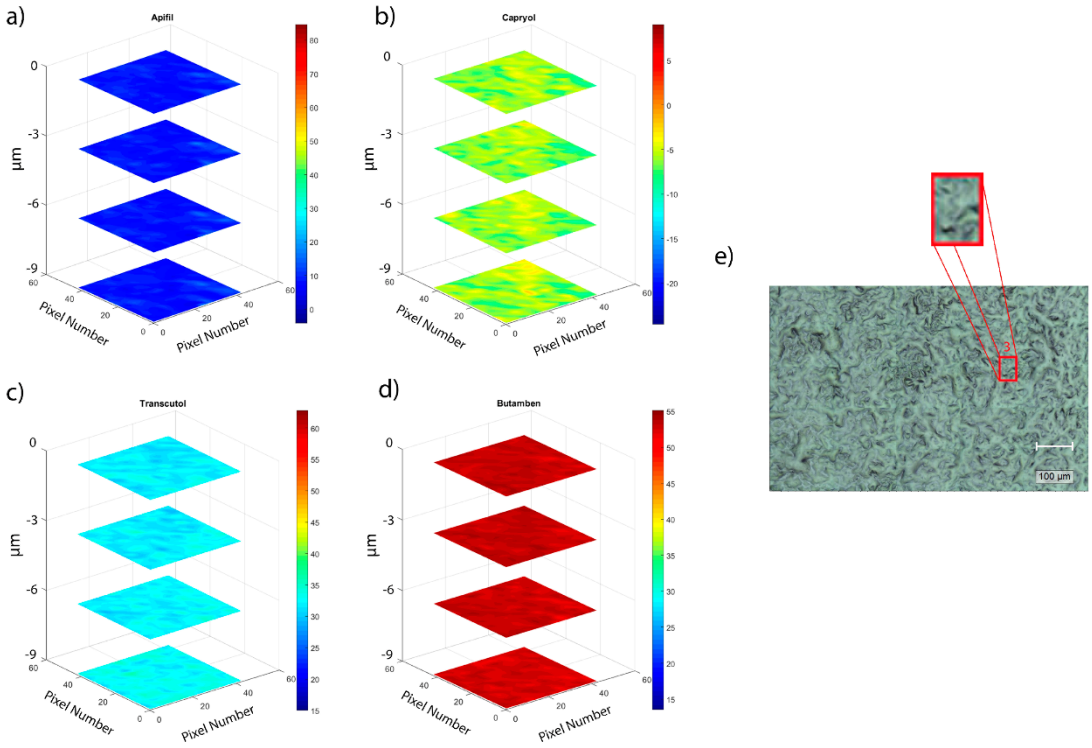

Figure S12. Volumetric Raman images obtained for a sample belongs to the homogeneous and rough surface category (AM4) in the region 3 (red square in (e)) for: a) Apifil®, b) Capryol® 90, c) Transcutol® and d) BTB (Scale bar = 100µm, *x* axis = 560 µm, *y* axis = 860 µm).

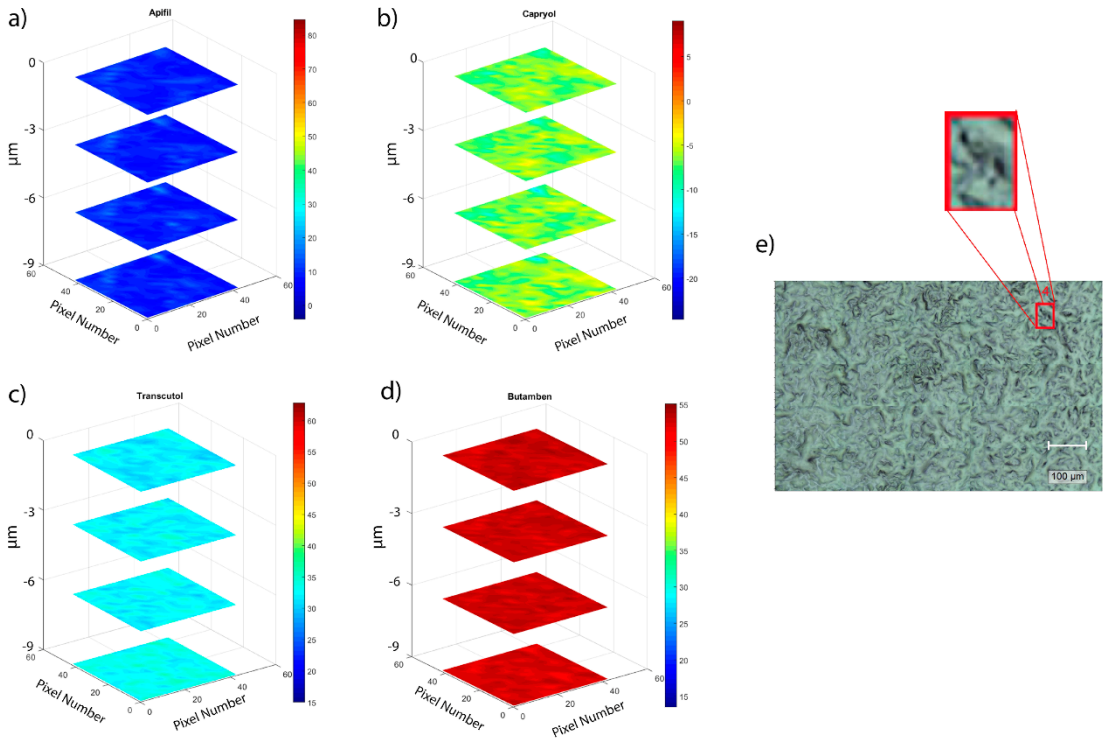

Figure S13. Volumetric Raman images obtained for a sample belongs to the homogeneous and rough surface category (AM4) in the region 4 (red square in (e)) for: a) Apifil®, b) Capryol® 90, c) Transcutol® and d) BTB (Scale bar = 100µm, *x* axis = 560 µm, *y* axis = 860 µm).

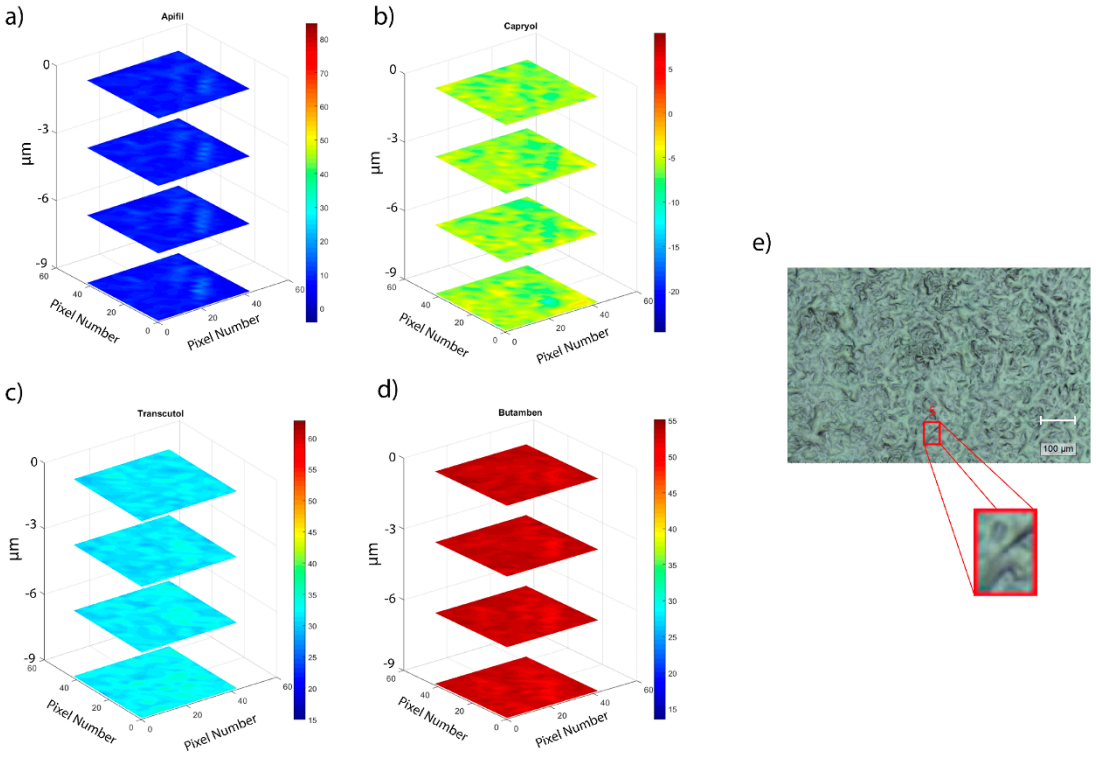

Figure S14. Volumetric Raman images obtained for a sample belongs to the homogeneous and rough surface category (AM4) in the region 5 (red square in (e)) for: a) Apifil®, b) Capryol® 90, c) Transcutol® and d) BTB (Scale bar = 100µm, *x* axis = 560 µm, *y* axis = 860 µm).

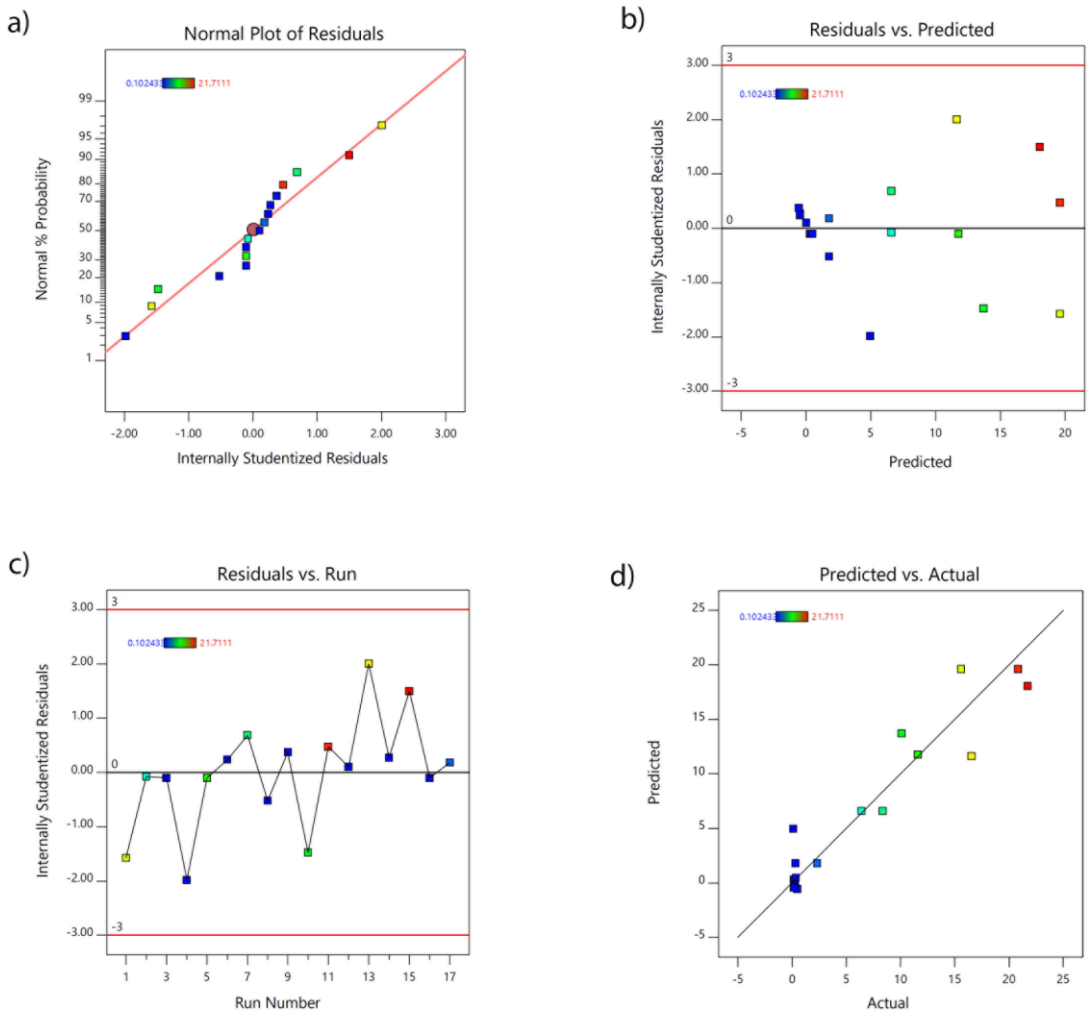

Figure S15. Diagnostic plots of STD_{map} Apifil: a) normal plot of residues, b) internally studentized residuals vs. predicted values, c) internally studentized residuals vs. Run number and d) predicted values vs. Experimental values.

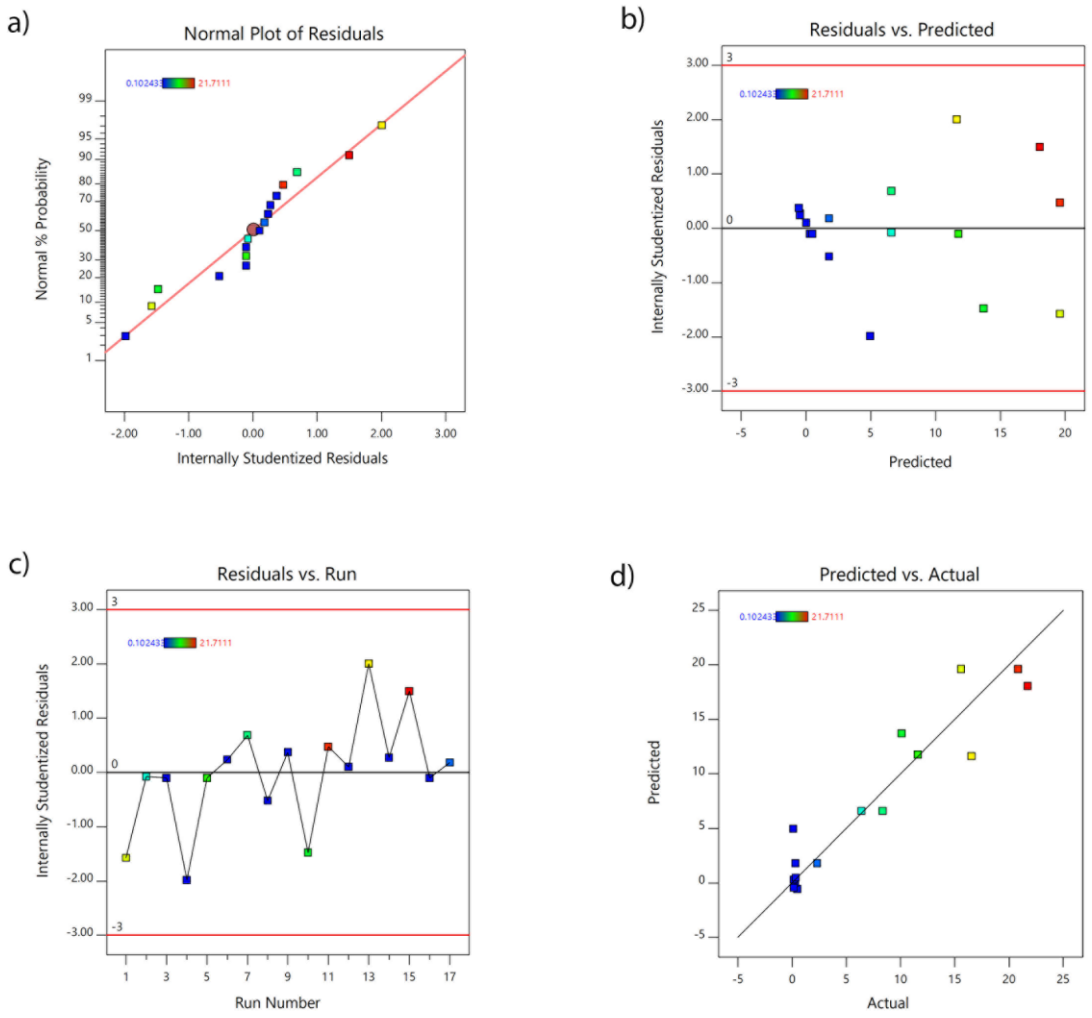

Figure S16. Diagnostic plots of STD_{map} Capryol® 90: a) normal plot of residues, b) internally studentized residuals vs. predicted values, c) internally studentized residuals vs. Run number and d) predicted values vs. Experimental values.

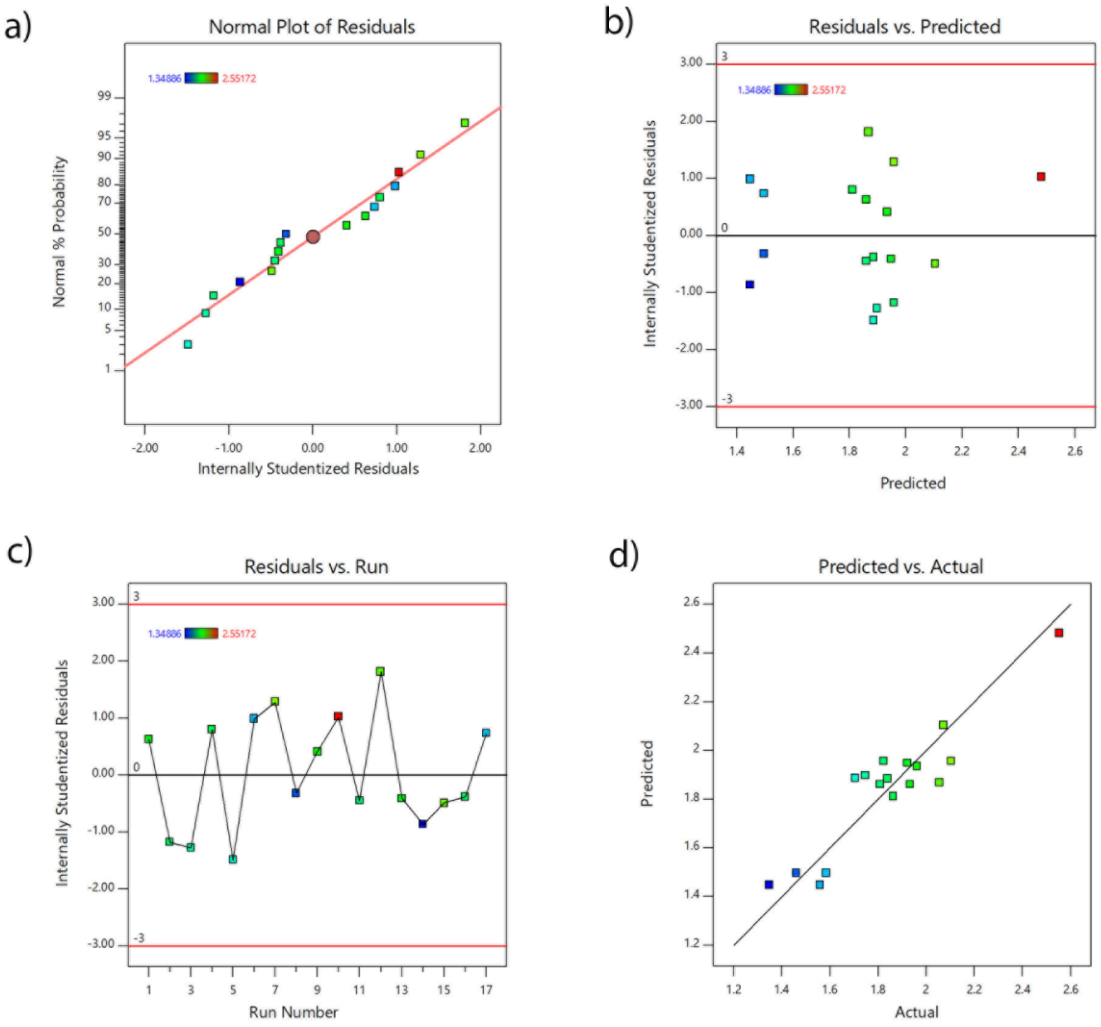

Figure S17. Diagnostic plots of DHI Capryol® 90: a) normal plot of residues b) internally studentized residuals vs. predicted values, c) internally studentized residuals vs. Run number and d) predicted values vs. Experimental values.

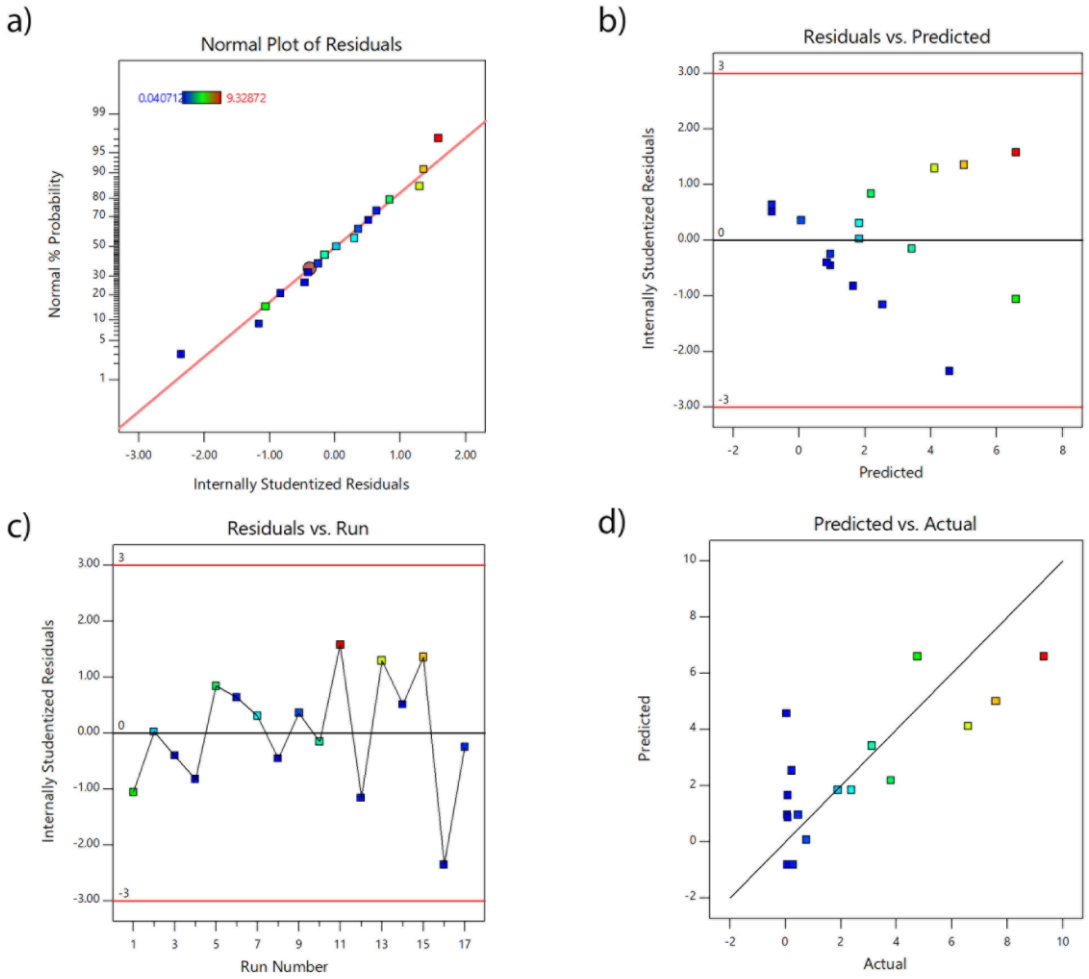

Figure S18. Diagnostic plots of STD_{map} BTB parameter: a) normal plot of residues, b) internally studentized residuals vs. predicted values, c) internally studentized residuals vs. Run number and d) predicted values vs. Experimental values.